Answers Research Journal 17 (2024): 677–707.
https://assets.answersresearchjournal.org/doc/v17/allosaurus_fragilis_skull.pdf

ARJ

Description and Analysis of an *Allosaurus fragilis* (Dinosauria: Theropoda) Skull

Nicholas Rush and C. L. Storm, Independent Scholars, Ohio

Abstract

CMP 279 is an *Allosaurus* specimen donated to the Creation Museum in Petersburg, Kentucky, United States, in 2013 and displayed in 2014. It includes a complete skull, hyoids, cervical vertebrae, sacral vertebrae, caudal vertebrae, chevrons, the dorsal portions of both left and right ilia, and the ventral part of the right femur. Notably, the most impressive feature of CMP 279 is its skull, which will be discussed in this description and attributed to the species *Allosaurus fragilis*. The basis for this classification includes:

1. The ventrally deflecting jugal.
2. The presence of two large pneumatic lacrimal openings that open laterally.
3. Tooth count which ranges between 66 and 78.
4. Slight rugosity on the dorsolateral margin of the nasal.

Comparative analyses were conducted with other *Allosaurus* specimens to ensure the accuracy of the species designation. Our description of CMP 279's cranial anatomy primarily relies on CT scans due to complications with the specimen's museum mounting. Additionally, we made in-person observations of accessible bones to supplement our findings from the CT scans. The use of CT scans allowed for a more precise identification of sutures, distinct from natural fractures and restoration work. This study also marks the first documented occurrence of neurovascular canals in *Allosaurus fragilis*. Furthermore, we identified a possible case of osteomyelitis on the anterior end of the right dentary. Several other potential pathologies were noted, including one on the left surangular, another on the opposing right surangular, and on the right lacrimal.

Keywords: *Allosaurus fragilis*, theropod, dinosaur, anatomical description, cranial anatomy, neurovascular canals, pathology, Morrison Formation, Jurassic

Introduction

In the year 2000, a property owner in Moffat County, Colorado, United States, made a remarkable discovery: exposed pieces of a dinosaur skeleton. The excavation of this skeleton took place between 2001 and 2002, revealing not only the skeleton itself but also one of the most complete *Allosaurus fragilis* skulls ever found. In 2013, this extraordinary find, both the skull and the rest of the skeleton, was generously donated to Answers in Genesis. The specimen was officially unveiled and put on display in 2014 at the Creation Museum located in Petersburg, Kentucky, United States.

Prior to its donation, the skull was informally named "Ebenezer," but from this point forward, it will be identified by its specimen number, CMP 279, which also pertains to the remainder of the skeleton. In 2017, as part of ongoing research efforts, computer tomography (CT) scans of the skull were conducted by James Berger and his colleagues at 3D Engineering Solutions, in Cincinnati, Ohio, United States.

Geologic Setting

The CMP 279 site is situated in Moffat County, Colorado, west of the town of Massadona and east of Dinosaur. It's approximately 76km southeast of the renowned Carnegie Quarry at Dinosaur National Monument. This site is a part of the Skull Creek Monocline, encompassing a section of dipping Jurassic and Cretaceous strata, ranging from the Nugget Sandstone to the Mancos Shale (Van Loenen and Bryant 1999; Whitmore and Snelling 2014).

In 2014, a preliminary study was conducted by a sedimentology and stratigraphy class from Cedarville University. They measured a portion of this geological section, commencing at the contact point between the Entrada Sandstone and Stump Formation and concluding at the junction of the Dakota Sandstone and Mancos Shale (fig. 1). The total thickness of the section they measured amounted to 193.6m, with the Morrison Formation constituting approximately 97.1m of this section (Anderson et al. 2014).

The Morrison Formation at this site comprises both the Salt Wash and Brushy Basin Members. The Salt Wash Member primarily consists of trough cross-bedded conglomeritic sandstones intermixed with reddish to gray mudstones. The Brushy Basin Member is primarily composed of red, gray, and purple mudstones with occasional siltstone, limestone, and sandstone lenses. It's worth noting that CMP 279 was discovered above 100m of the total section within the Brushy Basin Member. The specific layer in which CMP 279 was found is characterized by greenish-gray mudstone with minor glauconitic sandstone lenses (Anderson et al. 2014).

Fig. 1. (A) In the bottom right-hand corner an aerial map of the United States with the Skull Creek Monocline area in northwestern Colorado highlighted by the red square. The larger zoomed in aerial photo shows the CMP 279 site with the area of the measured section done by Anderson et al. (2014) highlighted by the red rectangle. The measured section starts at the contact of the Entrada Sandstone and Stump Formation. Then ending at the boundary between the Dakota Sandstone and Mancos Shale. The approximate location of the CMP 279 Quarry is marked by the red marker.

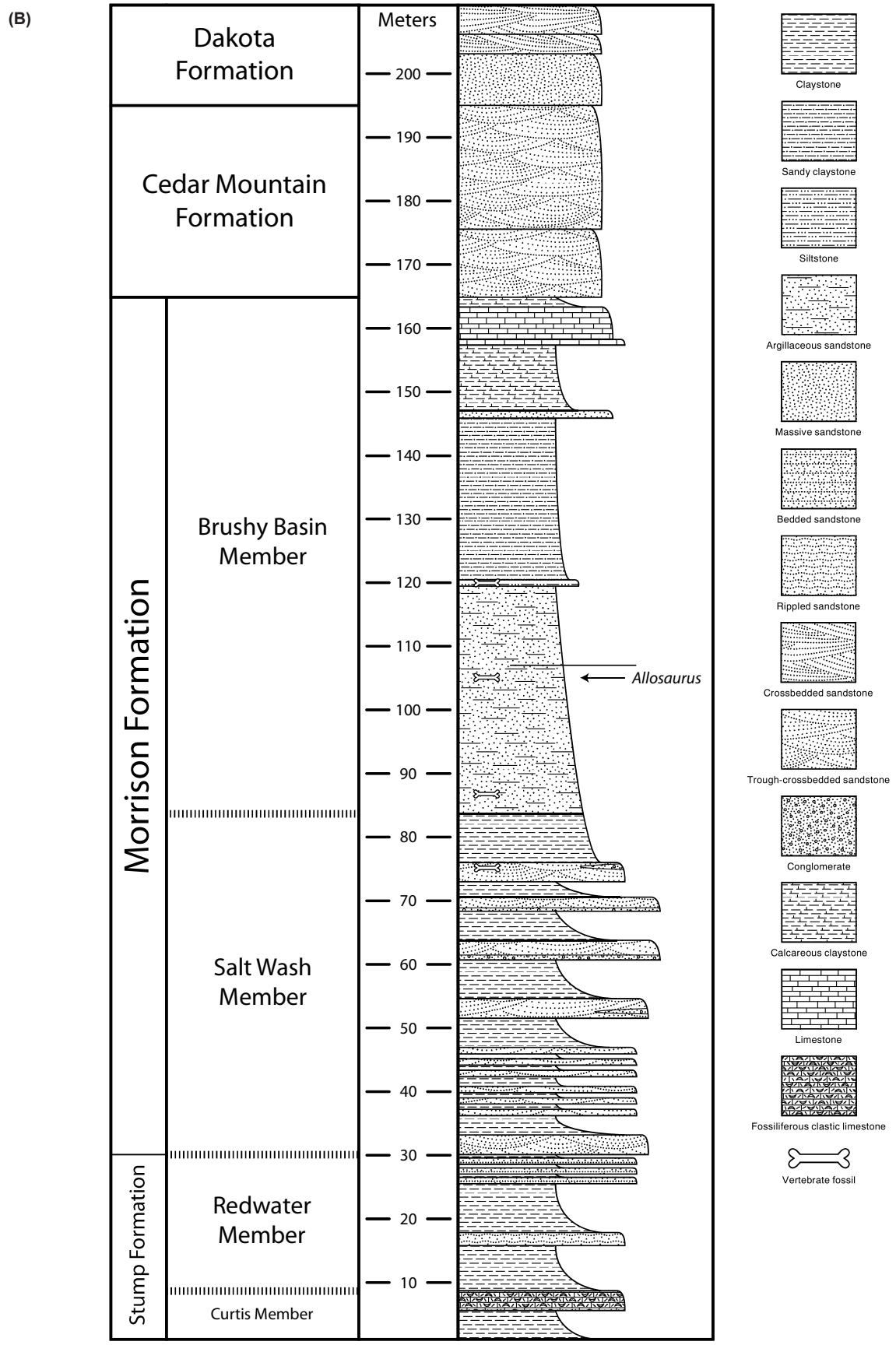

Fig. 1. (B) Stratigraphic and measured section from the CMP 279 site made by Anderson et al. (2014). The CMP 279 quarry is highlighted and occurs at about 105 m of the total section within the Brushy Basin Member of the Morrison Formation.

Species Designation

Class: Reptilia (Laurenti 1768)
Order: Saurichia (Seeley 1888)
Suborder: Theropoda (Marsh 1881)
Family: Allosauridae (Marsh 1878)
Genus: *Allosaurus* (Marsh 1877)
Species: *Allosaurus fragilis* (Marsh 1877)

CMP 279 demonstrates strong comparisons with other *Allosaurus fragilis* skulls, including the paratype skull at Dinosaur National Monument skull (DINO 2560) and the newly restored neotype skull at the United States National Museum of Natural History (USNM 4734) based on photographic evidence. A proposal put forth by Paul and Carpenter in 2010 aimed to designate USNM 4734 as the neotype for *Allosaurus fragilis*. This proposition arose due to the fact that the current holotype specimen, YPM 1930, consists of only a tooth, a dorsal centrum, two fragmentary caudal centra, a rib fragment, a proximal phalanx from the right pedal digit III, and a midshaft of the right humerus (Marsh 1877). The limited completeness of the YPM 1930 skeleton led both researchers to suggest the necessity for a more comprehensive specimen to aid in species diagnostics. Furthermore, the geographical proximity of USNM 4734, which originates from the same Garden Park quarry (Felch Quarry 1) to the current holotype adds weight to this proposition (Paul and Carpenter 2010). The researchers also emphasized the significance of the pathologies observed in USNM 4734 in understanding the behavior and life of theropod dinosaurs in general. Paul and Carpenter's proposal was finally accepted and the neotype is now USNM 4734 (International Commission on Zoological Nomenclature 2023)

USNM 4734 has been colloquially referred to as the short-snouted skull and has, by some accounts, been considered as representative of a different *Allosaurus* species than DINO 2560, known as the long-snouted skull. Robert Bakker, who supports this view, cites differences in morphology between the two skulls, including aspects like the laterotemporal fenestra and premaxilla (Bakker 1998). However, doubts were raised regarding whether the reconstruction of the USNM 4734 skull, conducted under the guidance of Charles Gilmore in the early 1900s, was done accurately (Carrano, Loewen, and Evers 2018; Madsen 1976). The skull was not initially found in an articulated state and underwent restoration by N.H. Boss following Gilmore's guidance (Gilmore 1920). Gilmore himself acknowledged making compromises in the rearticulation process, giving the skull its 'short-snouted' appearance (Carrano, Loewen and Evers 2018, Gilmore 1920). Carrano et al. (2018) later studied the disarticulated skull of USNM 4734 and found that its proportions matched those of DINO 2560. Additionally, a geometric morphometric analysis conducted by Carpenter in 2010 on *Allosaurus fragilis* skull elements from the Cleveland Lloyd Dinosaur Quarry identified two short-faced individuals, suggesting that these variations may represent extreme diversity within the species (Carpenter 2010). Considering that CMP 279 aligns with DINO 2560 in its proportions, and therefore can be compared to USNM 4734, this confirms CMP 279 is another specimen of *Allosaurus fragilis*. Any differences observed between CMP 279, DINO 2560, and USNM 4734 are more likely representative of intraspecific variation as suggested by Carpenter (2010) or, to a lesser extent, a subspecies, which is difficult to prove with only fossil evidence.

A prior species designation study conducted by Dr. Marcus Ross after CMP 279 was donated to Answers in Genesis in 2013 identified four criteria for distinguishing the species *Allosaurus fragilis*:

(1) the presence of a cornual process with two large pneumatic cavities that open laterally;
(2) the ventral margin of the jugal deflects ventrally at mid-length;
(3) tooth count matching that of *Allosaurus fragilis* (66-78); and
(4) the absence of neurovascular foramina in the maxilla ventral to the antorbital fenestra (Ross 2014).

The authors of this study concur with Dr. Ross's assessment of CMP 279 and, after comparing it to other specimens, place CMP 279 in the species *Allosaurus fragilis*. It should be noted, however, that we did observe the presence of foramina ventral to the antorbital fossa in the maxilla, a rare occurrence in *Allosaurus fragilis* and other allosauroids (Chure and Loewen 2020). Lastly, a final criterion that was not examined by Ross (2014), but by Chure and Loewen (2020) is amount of rugosity on the dorsolateral margin of the nasal. Chure and Loewen (2020) note that *Allosaurus fragilis* has slight rugosity along the dorsolateral margin of the nasal, while *Allosaurus jimmadseni* has a very rugose dorsolateral margin of the nasal. The rugosity on the nasals of *Allosaurus jimmadseni* forms a large bilateral crest (Chure and Loewen 2020). CMP 279 has a slight rugosity on the dorsolateral margin of the nasals that does not form a large bilateral crest. This is further confirmation that CMP 279 belongs to *Allosaurus fragilis*.

We would also like to note that the use of conventional systematics is not based on our approval of conventional taxonomy, but rather to match the conventional literature when a new specimen is described. We hope this brings open dialogue with those working in the conventional framework to include CMP 279 in the body of literature on *Allosaurus fragilis*. Outside the scope of this paper

a thorough baraminological analysis should be done to determine if the family Allosauroidea is a true holobaramin. To our knowledge a detailed baraminological analysis has only been done for a few therapod groups Tyrannosauroidea (Aaron 2014) and the clade Maniraptora (McLain, Petrone, and Speights 2018). Analyzing the family Allosauroidea will give us a better look into the created kind that includes *Allosaurus fragilis* and we look forward to those future studies.

Materials and Methods

In the typical process of creating a cranial anatomical description, direct in-person observations of the specimen are essential. However, various factors have made it challenging to conduct in-person observations for CMP 279. The skull is now permanently displayed, which has made certain areas, notably the palatine complex, inaccessible due to the mounting process. Additionally, the skull underwent extensive preparation to ensure it was in prime condition for display and conservation, making it difficult to distinguish between restored and original bone during in-person observations. These factors have led to a primary reliance on CT scans of the skull in compiling this description.

It is important to note that the CT scans of the skull are not complete due to limitations with the X-ray scanner (a Nikon XT H 450) used for the scans (fig. 2). While the scanner could accommodate the skull itself, its elongated shape meant that the x-ray source couldn't penetrate every part of the skull. As a result, the dorsal and ventroposterior sections of the skull were not fully scanned, leading to gaps in the imagery. The missing portions include the dorsoposterior part of the nasals and the dorsal segments of the lacrimals, prefrontals, frontals, parietals, squamosals, supraoccipitals, and postorbitals. Also absent from the scans are the ventral parts of the quadrates, pterygoid, and the quadratojugals. However, both mandibles were able to be completely scanned without complications. Furthermore, there were challenges related to the file size of the CT scans, which demanded a substantial amount of RAM for processing. To facilitate viewing of the cranial section, the scans had to be divided into 15 separate sections, making it challenging to follow a single suture, as multiple files had to be opened to ascertain its position. The file size remained substantial even after dividing it into sections, creating processing difficulties, especially when more RAM was allocated. Lastly, the dorsal section of the skull, which was too large for the scanner, resulted in less detailed shadowing in the areas close to the cutoff, making sutures more challenging to identify. In-person observations were consequently made in those areas where the CT scans were incomplete, focusing on accessible portions of the mounted skull.

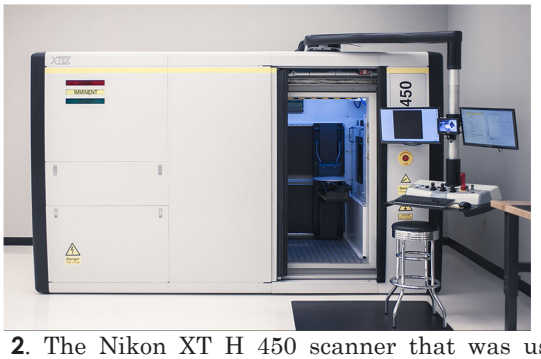

Fig. 2. The Nikon XT H 450 scanner that was used to create the CT scans. Photo courtesy of Answers in Genesis.

For this study, we employed MyVGL Viewer, a freely available volumetrics program. Upon opening the program, four panes become visible, with three representing each of the body planes (transverse, median, frontal), and the fourth pane displaying a 3D rendering of the bone (fig. 3). This 3D rendering allowed for the visualization of each scan's position and enabled manipulation of the rendering to alter the bone's orientation (fig. 4). Initial challenges in distinguishing fractures from sutures were addressed by referencing Madsen's 1976 *Allosaurus fragilis* monograph, which proved invaluable (fig. 5). In cases where difficulties persisted, Chure and Loewen's 2020 description of *Allosaurus jimmadseni* served as a helpful guide.

For each individual bone, the scans were examined in the three body planes, with careful attention to suture locations (fig. 6). Subsequently, a comparison was made to the corresponding bone on the right or left side. Descriptions of each bone followed "Romerian" terminology to detail its position (Romer 1956; Wilson 2006). Measurements were taken in centimeters using the software's caliper and line distance tools (fig. 7). It's important to acknowledge that CT scans are generally accurate up to 0.1 mm (Racicot 2016). However, due to the separation of the CT scans into sections for the cranial portion of the skull, measurements for this area may be less precise. In cases of in-person observations, calipers were used to take measurements of bones, fenestrae, and foramina in centimeters. Finally, the bones were compared to Madsen's monograph description of *Allosaurus fragilis* and to photographs of DINO 2560 and USNM 4734. Additional comparisons were drawn with the newly described *Allosaurus jimmadseni* (DINO 11541) and photographs of MOR 693, a specimen attributed to *Allosaurus jimmadseni*. When feasible, comparisons were also made with the European allosaur, *Allosaurus europaeus*. Two other species were chosen for comparison, namely *Acrocanthosaurus atokensis*, a carcharodontosaurid allosauroid, and *Ceratosaurus nasicornis*, a medium-

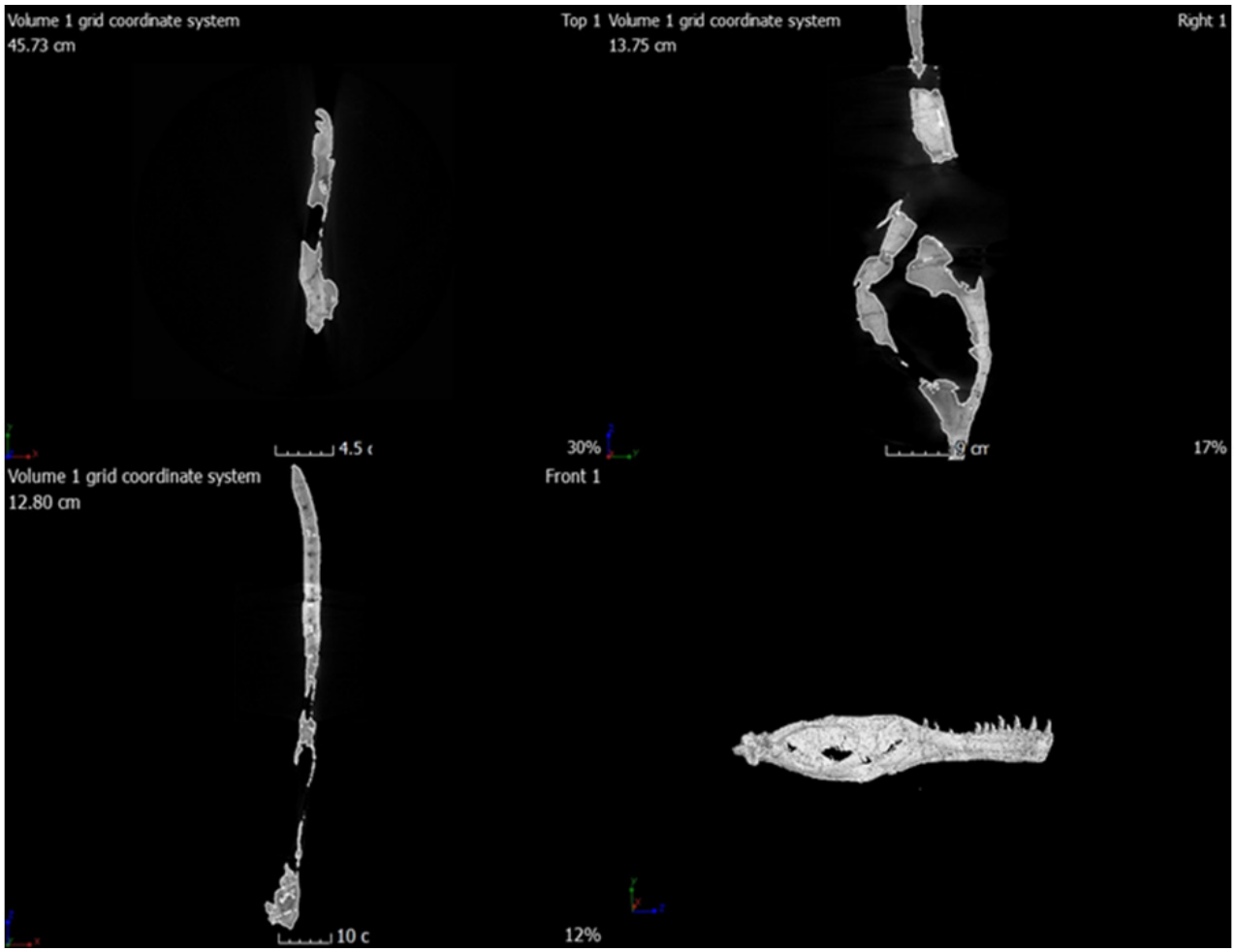

Fig. 3. The four panes that open when viewing the scans in MyVGL Viewer.

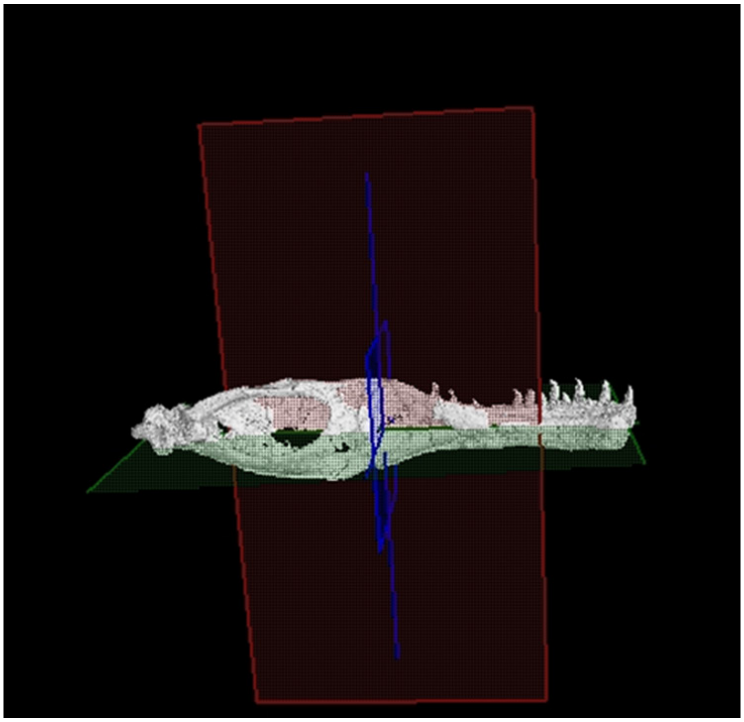

Fig. 4. This shows the position of the three body planes within the 3D rendering of the left mandible, green represents the transverse plane, red the median plane, and blue the frontal plane.

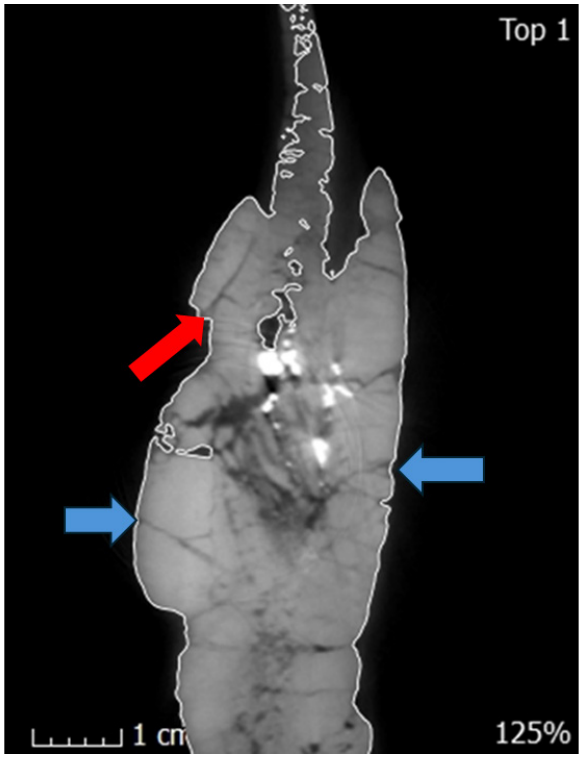

Fig. 5. A single CT slice of the left dentary in the internal frontal plane showing the suture (red arrow) between the supradentary and dentary and some fractures (blue arrows). These fractures are most likely stress fractures that resulted from compression of the skull after deposition. Sutures can be distinguished from these fractures based on their penetration distance. Fractures run for small distances while sutures run for longer distances. Combined with the anatomical descriptions from Madsen's 1976 monograph sutures were able to be determined.

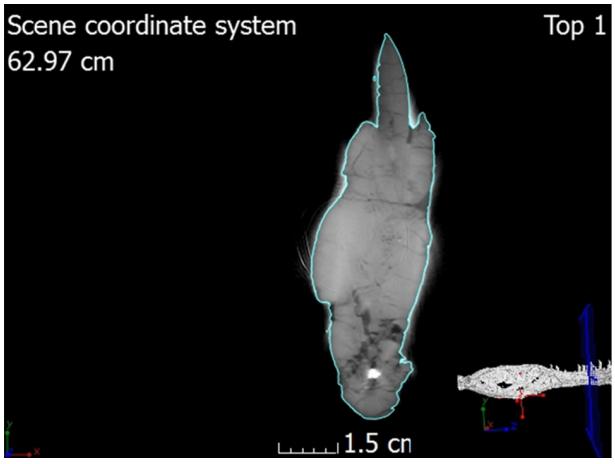

Fig. 6. A single CT slice of the left dentary showing the location of the scan within the 3D rendering.

sized non-tetanuran theropod also found within the Morrison Formation.

Skull Description

General Description of the Skull

The precise positioning of the skull and skeleton within the Brushy Basin Member remains uncertain. Historical records from the original dig site provide little to no definitive clues about its true orientation. While various accounts suggest that the skull was found lying on its right side, a photograph from the initial appraisal in 2003 indicates that it may have been positioned slightly on its left side, with the rostrum pointing into the hill (fig. 8) (Magovern 2003). The absence of orientation information in the photograph further complicates the understanding of the spatial placement of the skull and skeleton. Establishing this information would be valuable for gaining insights into the taphonomy and deposition of the site. Future sedimentological and taphonomic studies of the site could further shed light on these questions.

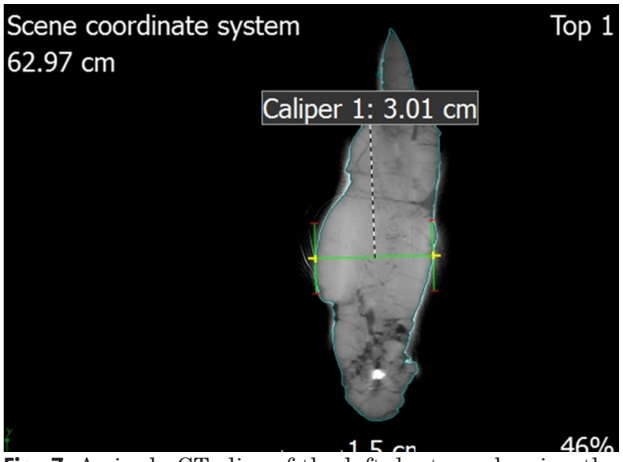

Fig. 7. A single CT slice of the left dentary showing the use of the caliper tool to take measurements.

Fig. 8. Photograph of the skull still in situ lying slightly on its left side from Magovern (2003).

Many of the cranial and mandibular elements of the skull are present, including the hyoids (fig. 9). However, the skull has sustained significant damage with both superficial and internal fractures. Before the preparation process, a substantial fracture ran dorsoventrally through the rostrum of the skull, affecting the right and left nasals, maxillae, and

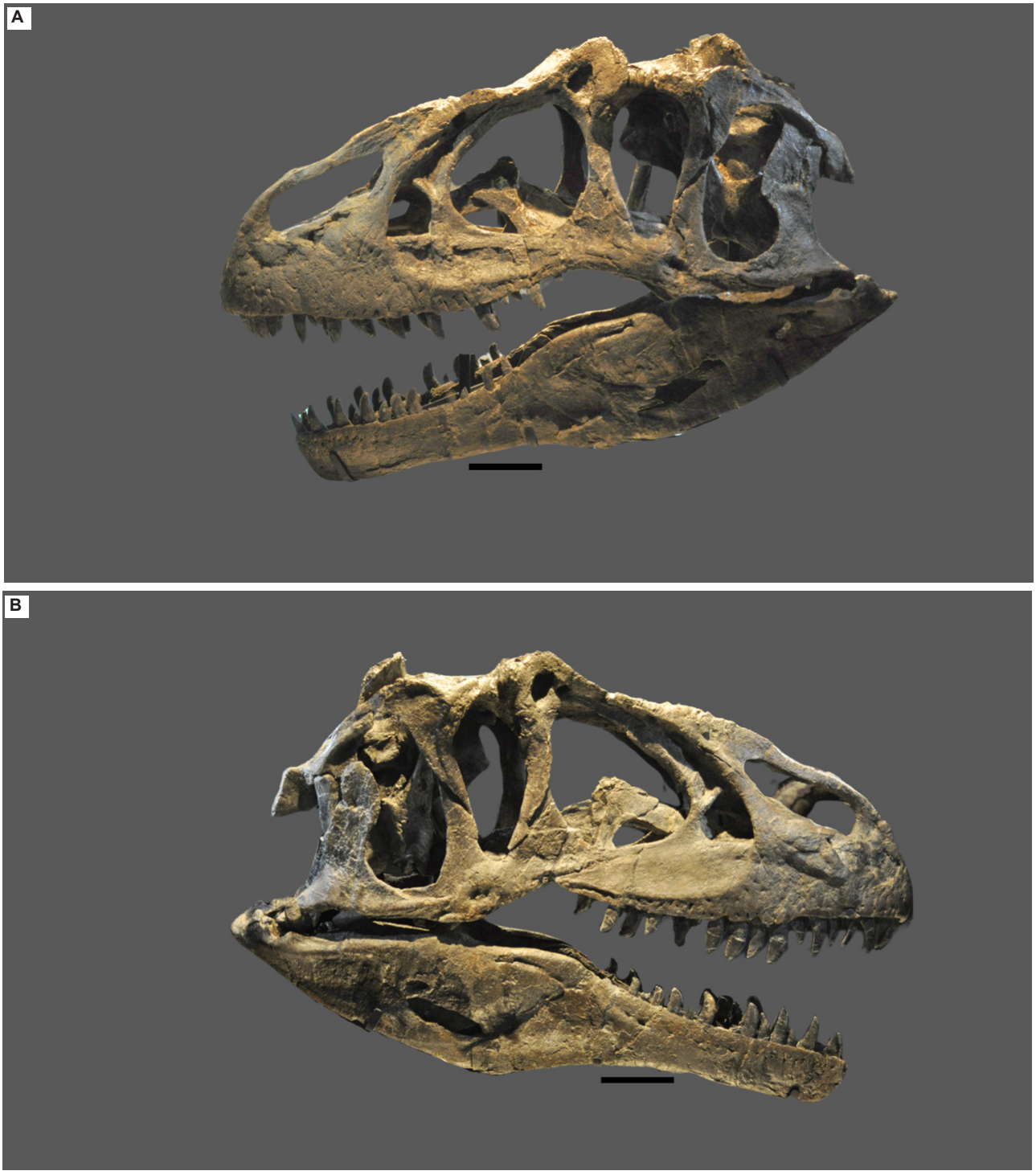

Fig. 9.(A) Left lateral view of the CMP 279 skull (Matt Petrone). (B) Right lateral view of the skull (Matt Petrone). Hyoids are not included in these photographs. Please refer to figs. 19 and 20. Scale bar is 10 cm.

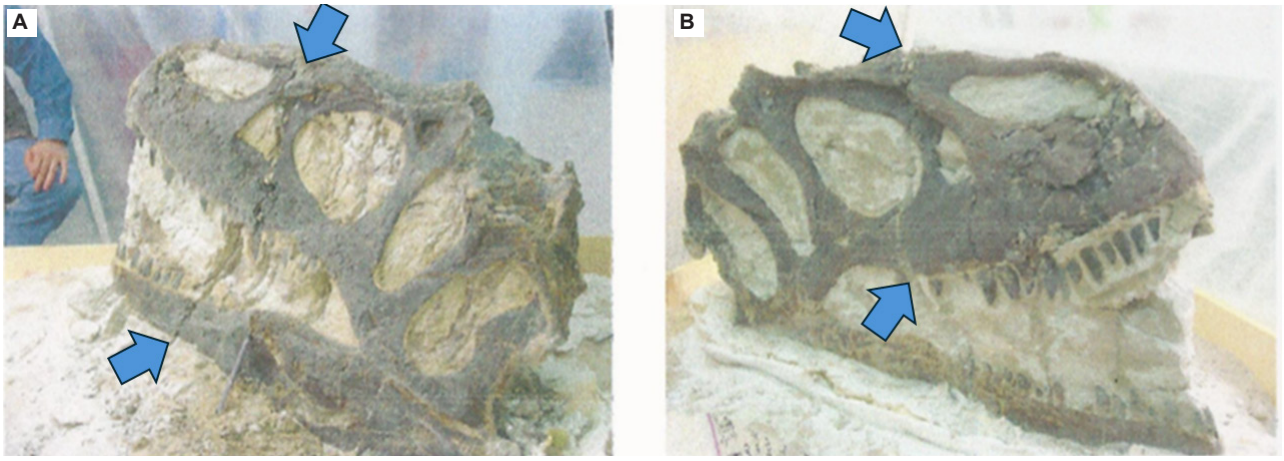

Fig. 10. (A) The large fracture in left lateral view highlighted by arrows from Magovern (2003). (B) The large fracture in right lateral view highlighted by arrows from Magovern (2003).

dentaries (fig. 10). This fracture caused the rostrum to become slightly detached from the rest of the cranium, resulting in a more ventrally depressed appearance. The repair work done to mend this fracture is visible in the scans (fig. 11). The skull has also experienced lateral compression on the right side, giving it an overall thinner appearance. This compression led to a fracture that runs dorsoventrally through the jugal and surangular. Furthermore, the right side of the rostrum is more dorsally upturned as a consequence of this compression, observable in the dorsal margin of the right nasal and right lacrimal crest. Both bones

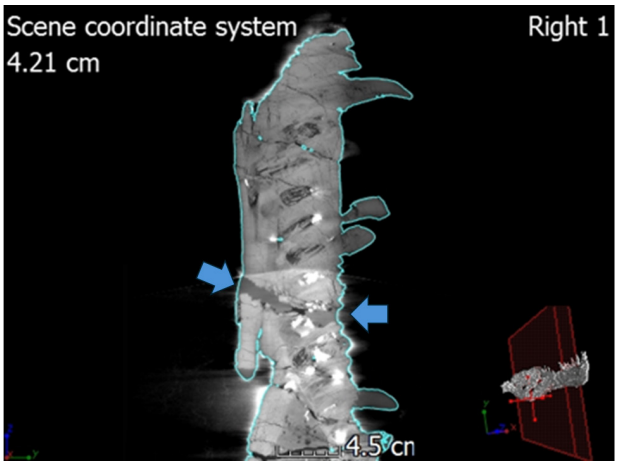

Fig. 11. A single slice of CT scan of the left dentary in internal lateral view showing the restoration work that was done to repair the large fracture.

appear slightly compressed medially, giving them a flatter appearance compared to their counterparts on the left side (fig. 12).

The skull is approximately 97% complete, with only a few missing teeth from the cranium and mandibles. After some investigation, it was found that the vomer is absent, and regrettably, the most plausible explanation is that the vomer was destroyed during the preparation process. The stapes, which

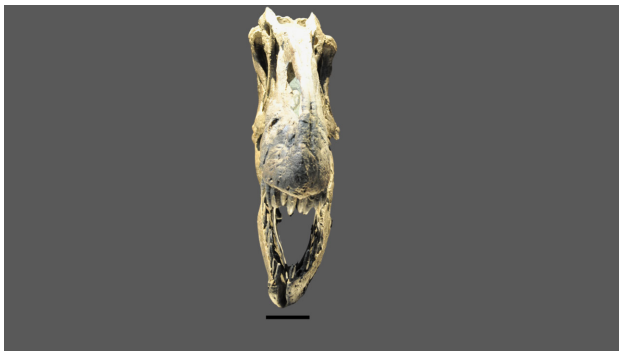

Fig. 12. The skull of CMP 279 in anterior view showing the dorsally upturned portions on the right side and undistorted left side (Matt Petrone). Scale bar is 10 cm.

is a thin, delicate, rod-like bone, is also absent. It remains unclear whether this absence is a result of the preparation process or if the bone was removed during the taphonomic processes. The delicate nature of the stapes bone means that it is typically missing from most *Allosaurus fragilis* specimens. However, it has been documented in specific cases such as UNHM VP 16605 and 16606, as well as in *Allosaurus jimmadseni* specimens like DINO 11541 and MOR 693 (Chure and Loewen 2020: Madsen 1976). There are a total of 54 exposed teeth, distributed as follows: 16 in the right premaxilla/maxilla, 13 in the left premaxilla/maxilla, 14 in the right dentary, and 11 in the left dentary. The average length of exposed teeth, measured from the crown to root, is about 7.9 cm. The number of teeth in *Allosaurus fragilis* can vary depending on the number of dental alveoli present (Madsen 1976). The overall length of the cranium, from the anterior edge of the premaxilla to the posterior edge of the quadrate, measures approximately 86.36 cm (tables 1 and 2). The overall height of the cranium, from the ventral edge of the left jugal to the dorsal edge of the left lacrimal, is approximately 30.91 cm. Specific mandibular lengths are provided in table 3 (see tables 3 and 4). Due to

Table 1. Measurements for the bones of the cranium. The height measurements for the quadrate and parietal could not be taken due to the museum mounting.

Left Side	Height (cm)	Width (cm)	Length (cm)
Premaxilla	25.81	2.51	12.85
Nasal	2.93	2.20	39.06
Maxilla	26.19	2.58	50.53
Lacrimal	23.46	7.0	26.0
PreFrontal	4.4	4.5	10.5
Frontal	4.2	9.7	12.5
Postorbital	15.63	5.89	17.33
Jugal	14.58	1.10	13.63
Squamosal	15.21	12.16	25.70
Quadratojugal	13.5	2.70	24.10
Quadrate	-	8.40	21.0
Parietal	-	15.50	5.70
Palatine	12.78	3.36	6.89
Pterygoid	7.43	0.94	33.86
Ecotpterygoid	3.02	6.15	1.90
Right Side	**Height (cm)**	**Width (cm)**	**Length (cm)**
Premaxilla	23.04	2.89	12.40
Nasal	2.13	3.30	39.53
Maxilla	26.20	3.21	49.03
Lacrimal	26.19	5.9	26.50
PreFrontal	1.90	4.50	9.90
Frontal	3.9	10.30	11.40
Postorbital	15.85	6.13	17.42
Jugal	13.03	1.14	13.28
Squamosal	16.24	12.25	25.62
Quadratojugal	13.20	2.90	19.00
Quadrate	-	6.10	19.50
Parietal	-	8.40	7.20
Palatine	13.82	4.45	6.52
Pterygoid	7.39	0.76	36.11
Ecotpterygoid	3.15	6.96	1.66

its uncompressed state, measurements taken from the left side of the skull are considered more likely to be accurate than those taken from the right side of the skull (figs. 13 and 14). Illustrations are included in the paper to enhance understanding and provide visual clarity for readers (please reference figs. 15–18).

Description of the Cranium

Premaxillae

The premaxilla body exhibits a rectangular shape, appearing more boxy in *Allosaurus fragilis* than in *Allosaurus jimmadseni*, which tends to have a slightly more elongated anterior portion (Chure and Loewen 2020). In lateral view, the nasal process of the premaxilla extends dorsally from the rest of the premaxilla body. In medial view, the maxillary process meets the maxilla dorsomedially. Both processes create a large notch forming the anterior edge of the external naris. The angle of the nasal process seems to display variability among *Allosaurus fragilis* specimens. Carpenter (2010) observed variations in the shape and size of the premaxilla, leading to different appearances of individuals with either short or long rostrum. This variation is partly due to the angle of the nasal process. In the case of CMP 279, the angle measures approximately 117° and appears to closely match that of DINO 2560 and USNM 4734 in photographs. Within the Cleveland-Lloyd premaxilla, the angle variation resulted in acute angles with a gently sloping process, as seen in *Ceratosaurus nasicornis*, or an obtuse angle, resembling *Acrocanthosaurus atokensis* (Carpenter 2010; Eddy and Clarke 2011; Madsen and Welles 2000).

Along the ventral margin of the external naris there is a flattened surface located midway along the premaxilla body, known as the narial fossa. At the point of contact between the premaxilla and maxilla, a small notch within the narial fossa is referred to as the perinarial fossa. As noted in Eddy and Clarke (2011), the premaxilla body of *Allosaurus fragilis*, in general, is longer than it is tall, in contrast to

Table 2. Measurements for the major fenestra and foramina of the cranium.

Left Fenestra and Foramina	Height (cm)	Width (cm)
Nasal Fenestra	5.7	19.5
Antorbital Fenestra	19.5	20.5
Orbital Fenestra	21.75	11.9
Laterotemporal Fenestra	21.9	8.0
Supratemporal Fenestra	7.6	9.8
Maxillary Fenestra	7.4	5.9
Nasal Foramen (Dorsal)	1.8	2.5
Nasal Foramen (Ventral)	0.8	1.2
Perinarial Fossa	1.8	1.7
Lacrimal Vacuity	4.9	4.5
Foramen Magnum	**Height (cm)**	**Width (cm)**
	3.4	**2.9**
Right Fenestra and Foramina	**Height (cm)**	**Width (cm)**
Nasal Fenestra	2.7	19
Antorbital Fenestra	20.0	20.5
Orbital Fenestra	21.6	8.7
Laterotemporal Fenestra	23.0	8.0
Supratemporal Fenestra	7.2	7.6
Maxillary Fenestra	6.7	6.8
Nasal Foramen (Dorsal)	1.6	3.9
Nasal Foramen (Ventral)	0.9	1.9
Perinarial Fossa	1.6	1.6
Lacrimal Vacuity	4.2	4.9

Table 3. Measurements of the mandibular bones.

Left Mandible	**Thickness (cm)**	**Height (cm)**	**Length (cm)**
Dentary	2.79	8.09	49.73
Angular	0.68	4.13	58.68
Surangular	0.85	9.10	31.65
Articular	3.85	2.79	6.50
Splenial	0.57	10.59	29.79
Prearticular	0.80	15.03	42.66
Supradentary	0.42	1.74	32.06
Coronoid	0.26	5.30	8.80
Antarticular	3.80	7.02	3.66
Right Mandible	**Thickness (cm)**	**Height (cm)**	**Length (cm)**
Dentary	3.08	8.10	51.79
Angular	1.54	5.64	57.27
Surangular	1.38	10.14	30.36
Articular	4.33	5.35	7.39
Prearticular	0.92	16.44	41.19
Splenial	0.49	10.47	31.13
Supradentary	0.51	1.61	32.75
Coronoid	0.39	5.10	8.37
Antarticular	1.28	4.82	2.76
	Total Length of Left Mandible (cm):~108.41		Total Length of Right Mandible (cm):~109.06

Table 4. Measurements of the external mandibular foramen in the right and left mandibles.

External Mandibular Foramen	**Height (cm)**	**Width (cm)**
Left Mandible		
External Mandibular Foramen	4.21	18.03
Right Mandible		
External Mandibular Foramen	3.87	12.78

Acrocanthosaurus atokensis, which is taller than long. Along the ventral margin, there is a linear row of foramina that extends anteroposteriorly. Additionally, scattered foramina can be found ventral to the narial fossa, which likely serve as outlets for the medial ethmoidal nerve and subnarial artery (Chure and Loewen 2020; Eddy and Clarke 2011).

Maxillae

The maxilla is the largest bone in the dermatocranium of *Allosaurus fragilis*. In lateral view, its contact with the posterior margin of the premaxilla is nearly vertical. At this juncture, the maxilla forms the posterior edge of the perinarial fossa, contributing to the overall structure.

The nasal process of the maxilla rises to meet the nasal bone at an angle of about 50°, which differs from the 35° angle reported in *Allosaurus jimmadseni* (Chure and Loewen 2020). Notably, this angle is more in line with that found in *Ceratosaurus nasicornis*. In contrast, *Acrocanthosaurus atokensis* resembles *Allosaurus jimmadseni* with a 40° angle based on a rough measurement of the right maxilla illustration (Eddy and Clarke 2011; Madsen and Welles 2000). It is worth mentioning that the holotype of *Allosaurus jimmadseni* (DINO 11541) is skeletally immature but more complete compared to MOR 693, which features an angle of 50°, similar to CMP 279 (Chure and Loewen 2020). This suggests that this angle may change ontogenetically, or there could be some variation among *Allosaurus jimmadseni* individuals. The likelihood of ontogenetic changes in this angle is supported by the angle of IPFUB Gui Th 4, a hatchling allosaurid from Portugal, which measures 40° based on the illustration of the maxilla (Rauhut and Fechner 2005). This ontogenetic change could correspond with the lengthening of the rostrum.

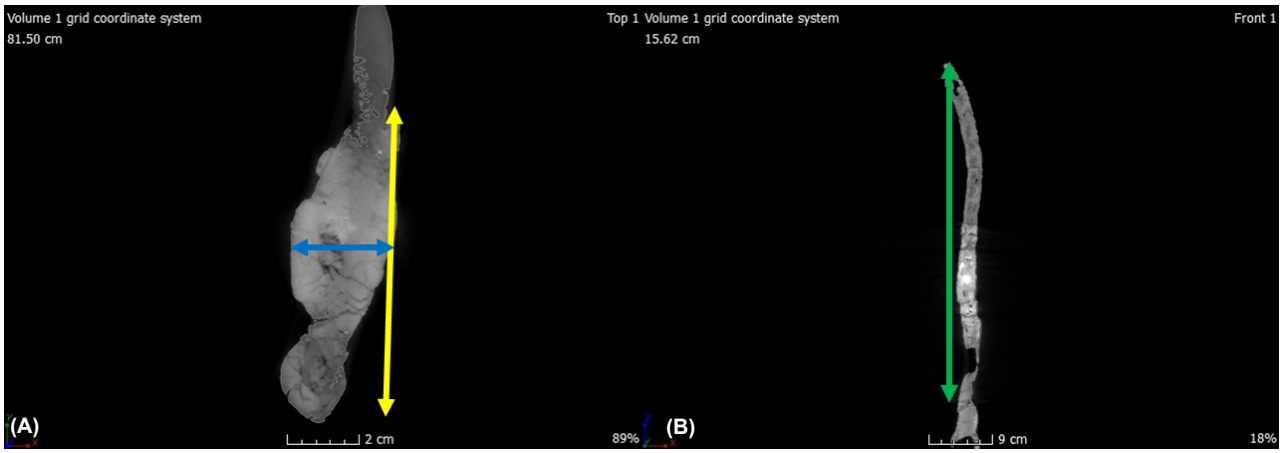

Fig. 13. (A) A single CT slice of the left dentary in internal frontal view shows how measurements were taken. The yellow arrow represents the height, measured at the middle section of each bone. The blue arrow represents the width, also measured at the middle section of each bone. (B) A single CT slice of the left dentary in internal dorsal view with the green arrow that represents the full length taken for each bone.

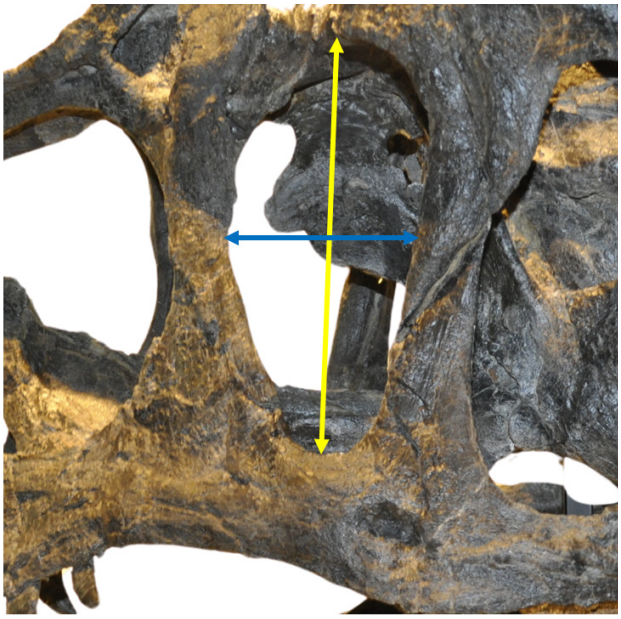

Fig. 14. Left lateral view of the orbital fenestra showing how measurements were taken for the fenestra and foramen. The yellow arrow represents the height, measured at the longest section, usually in the middle of the fenestra or foramen. An exception is the height of the antorbital fenestra, where the measurement was taken diagonally to capture the longest dimension. The blue arrow represents the width, typically measured from the center.

Continuing in lateral view, the maxilla forms the largest and anteriormost part of the antorbital fenestra. The dorsal surface of the maxilla is smooth and slightly laterally depressed, and this surface serves as the ventral margin of the antorbital fossa. The antorbital fossa is the likely site for the extension of the paranasal air sinus, specifically the sinus (Witmer 1997a, 1997b). Ventral to the ventrolateral surface of the antorbital fenestra, there is a row of foramina that punctuate the length of the maxilla. These foramina continue to pepper the ventral surface of the maxilla going anteriorly.

Nasals

The nasal is a thin, elongate bone forming the dorsal margin of the external naris. In lateral view the anterior portion of the nasal process contacts the premaxilla at a shallow angle going from posterior to anterior dorsoventrally. The nasal along with the lacrimal, forms the dorsal margin of the antorbital fossa. Ventrally below the highest rugosity of the nasals are two pneumatic foramina with the dorsal foramen being the smallest of the two. The number of pneumatic foramina appears to vary among different *Allosaurus* species and within *Allosaurus fragilis*, as well. DINO 11541 has a singular large foramen while MOR 693 has three (Chure and Loewen 2020). ML 415 (*Allosaurus europaeus*) has two foramina similar to CMP 279, while the more dorsal foramen is the largest (Mateus 2006). Madsen (1976) only includes a single large foramen in his composite monograph. It is uncertain whether Madsen included only a single nasal foramen in his composite or if it was observed in an actual specimen.

The nasal overlaps the maxilla forming a shallow angle that goes from posterior to anterior

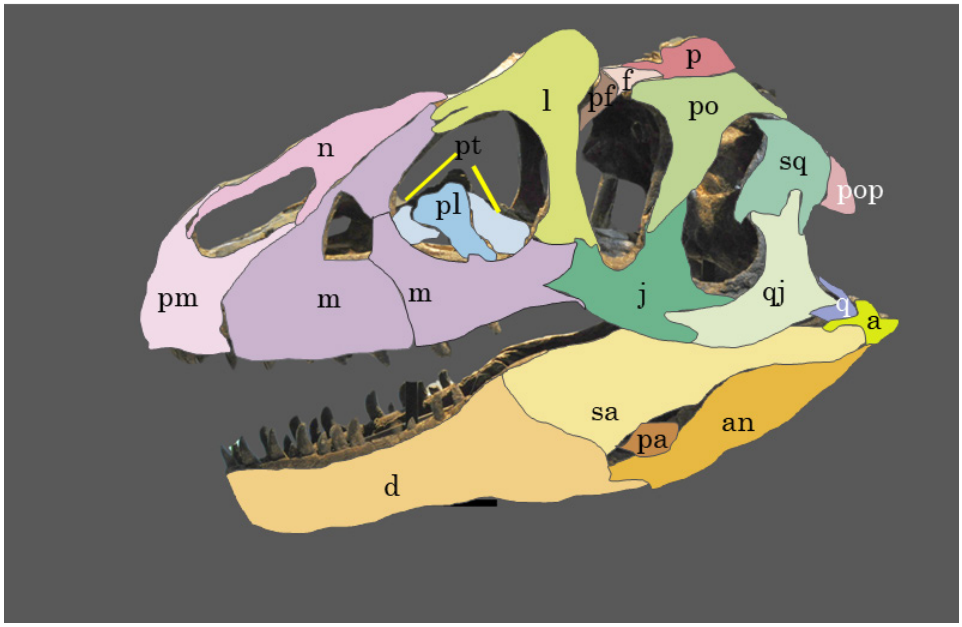

Fig. 15. Explanatory line drawing of CMP 279 in left lateral view showing the major bones of the cranium and mandible. Osteological abbreviations: a, articular; an, angular; d, dentary; f, frontal; j, jugal; l, lacrimal; m, maxillary; n, nasal; p, parietal; pa, prearticular; pf, prefrontal; pl, palatine; pm, premaxilla; po, postorbital; pop, paroccipital process (exoccipital); pt, pterygoid; q, quadrate; qj, quadratojugal; sa, surangular; sq, squamosal.

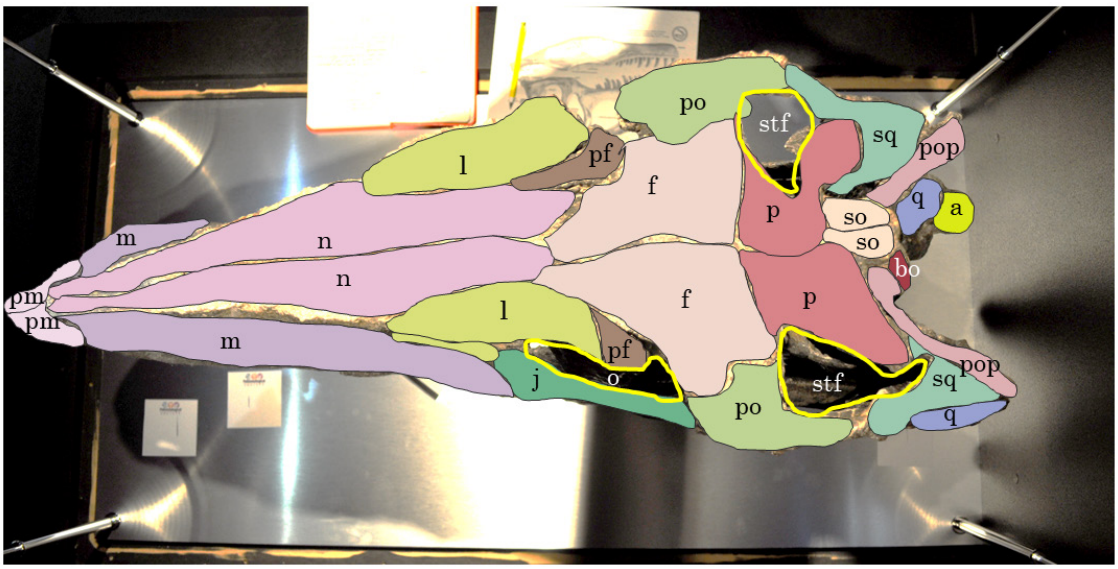

Fig. 16. Explanatory line drawing of CMP 279 in ventral view showing the ventral surface of the cranium. Osteological abbreviations: a, articular; bo, basioccipital; f, frontal; j, jugal; l, lacrimal; m, maxillary; n, nasal; o, orbital fenestra; p, parietal; pf, prefrontal; pl, palatine; pm, premaxilla; po, postorbital; pop, paroccipital process (exoccipital); pt, pterygoid; q, quadrate; so, supraoccipital; sq, squamosal; stf, supratemporal fenestra.

dorsoventrally. On the lateral side, the nasal process overlaps the premaxilla's nasal process, while on the medial side, the subnarial process of the nasal overlaps the premaxilla's nasal process. These interactions create a small notch that provides support to the nasal process of the premaxilla. This is also seen in *Allosaurus jimmadseni* and *Acrocanthosurus atokensis* (Chure and Loewen 2020; Eddy and Clarke 2011). This is also the case for *Ceratosaurus nasicornis;* however, since both the supranarial process and the nasal processes are shorter, the contact angle is steeper and at the contact the nasal process flares out laterally (Madsen and Welles 2000). The medial symphysis is well defined and separates the left and right nasals. Internally this surface is smooth and long probably,

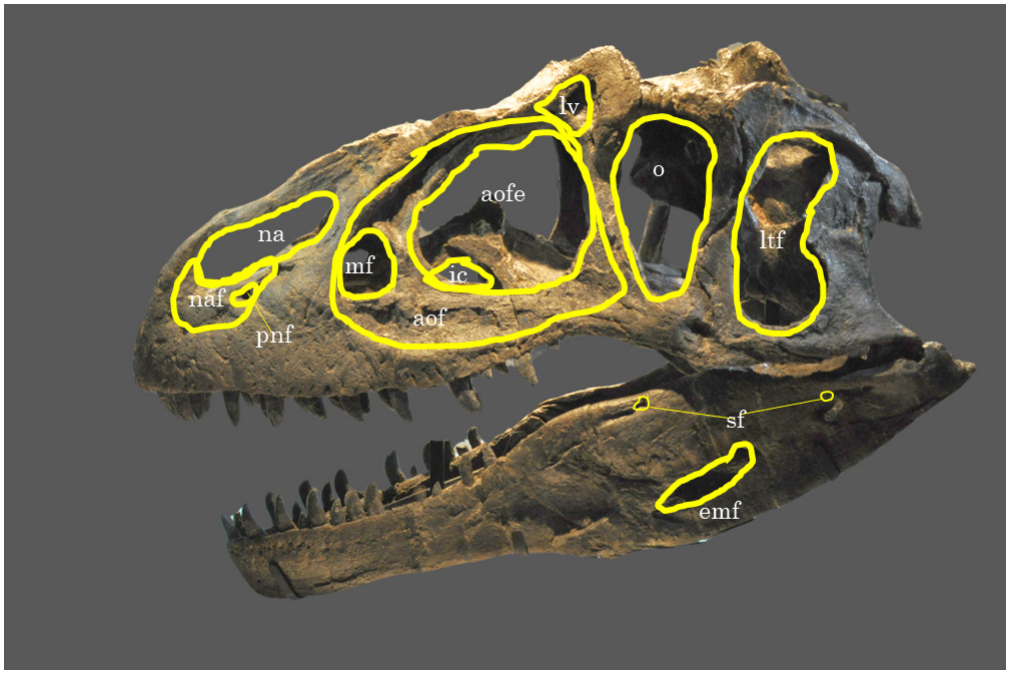

Fig. 17. Explanatory line drawing of CMP 279 in left lateral view showing the location of major fenestra and foramen. Osteological abbreviations: aof, antorbital fossa; aofe, antorbital fenestra; emf, external mandibular foramen; ic, internal choanae; ltf, laterotemporal fenestra; lv, lacrimal vacuity; mf, maxillary fenestra; na, naris; narial fossa (external naris); o, orbital fenestra; sf, surangular foramen.

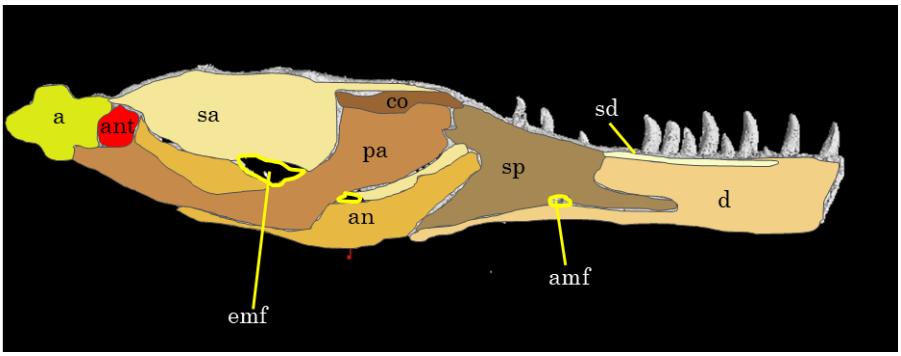

Fig. 18. Explanatory line drawing of CMP 279 of the left mandible in medial view. The image comes from the 3D rendering of the left mandible in MyVGL viewer since the bones are not accessible due to the museum mounting of the skull. Osteological abbreviations: a, articular; amf, anterior mylohyoid foramen; an, angular; ant, antarticular; c, coronoid; d, dentary; emf, external mandibular foramen; pa, prearticular; sa, surangular; sd, supradentary; sp, splenial.

indicating a loose internasal contact similar to that of *Allosaurus jimmadseni* and *Acrocanthosaurus atokensis atokensis* (Chure and Loewen 2020; Eddy and Clarke 2011). The dorsal surface of the nasal is smooth but going laterally from the medial symphysis the margin of the nasal has a rugose texture. In *Allosaurus jimmadseni* this rugosity forms a bilateral crest that is highest anteriorly to the cornual process and lowest at the nasal's anterior margin (Chure and Loewen 2020). In CMP 279 this rugosity is not as defined as *Allosaurus jimmadseni* and the right nasal has an exaggerated appearance due to its compressed nature. The left nasal exhibits the highest rugosity dorsally above the lacrimal/nasal suture and lowest at the nasal's anterior margin. USNM 4734 (*Allosaurus fragilis*) and *Allosaurus europaeus* also have this defined rugosity, but no rugosity is present in one specimen (DINO 2560), making it similar to *Acrocanthosaurus atokensis* and *Ceratosaurus nasicornis* (Eddy and Clarke 2011; Madsen and Welles 2000; Mateus 2006). Plate 2 of Madsen's monograph (1976) showing the composite skull in dorsal view demonstrates there can be different levels of rugosity: smooth (left nasal) also like DINO 2560 or very rugose (right nasal) also like CMP 279 and USNM 4734.

Lacrimals

The lacrimal is an ear shaped bone with a large fossa that opens laterally. This fossa is the lacrimal vacuity a pneumatic recess, which is a continuation of the pneumatic excavation of the antorbital fenestra, which is deeply excavated anteroposteriorly. Gilmore (1920) notes that there is variation in the size and shape of the vacuity and notes that there can be two openings. Both lacrimals of CMP 279 have two openings to the lacrimal vacuity. This is also seen in USNM 4734 but not in DINO 2560. The presence of two openings is similarly seen in *Acrocanthosaurus atokensis*, but this is not noted in any of the specimens of *Allosaurus jimmadseni* (Chure and Loewen 2020; Eddy and Clarke 2011). Ventral to the lacrimal vacuity is the canalis nasolacrimalis or nasolacrimal duct, a small foramen that acts as a connection between the antorbital and orbital fenestra.

In lateral view, the lacrimal makes up the dorsal most part of the antorbital fenestra and the anterodorsal most part of the orbital fenestra. Continuing in lateral view, the anterior lacrimal ramus overlaps the postdorsal ramus of the maxilla ventrally beneath the contact of the lacrimal and nasal. This is similar to *Acrocanthosaurus atokensis*, *Ceratosaurus nasicornis*, and *Allosaurus jimmadseni* (Chure and Loewen 2020; Eddy and Clarke 2011; Madsen and Welles 2000). At the lacrimal's most ventral portion the lacrimal contacts the maxilla again at its most posterior portion within the antorbital fenestra. Here the lacrimal also contacts the dorsal surface of the anterior portion of the jugal. This is the same for *Allosaurus jimmadseni* and possibly *Ceratosaurus nasicornis* (Chure and Loewen 2020; Madsen and Welles 2000). This differs in *Acrocanthosaurus atokensis* and *Allosaurus europaeus*, where the lacrimal does not contact the maxilla a second time, but instead the jugal takes up the entire space making up more of the ventrolateral surface of the antorbital fenestra than in *Allosaurus* (Eddy and Clarke 2011; Mateus 2006).

Prefrontals

The prefrontal is a small crescent-shaped bone. In dorsal view, the prefrontal sits medially behind the lacrimal. The medial edge of the prefrontal contacts both the lateral edges of both the nasal and frontal. Chure and Loewen (2020) note that the prefrontal in *Allosaurus jimmadseni* is indistinguishable from the prefrontal of *Allosaurus fragilis*. In *Acrocanthosaurus atokensis* however the prefrontal is splint-like and contacts the anterior edge of the postorbital (Eddy and Clarke 2011).

Frontals

The frontal is a wedge-shaped bone that makes up one of the dorsal margins of the orbital and anterior most margin of the supratemporal fossa and fenestra. In dorsal view the surface of the frontal is smooth and articulates with the prefrontal, postorbital, nasal, and parietal. The contact with the nasal is slightly interdigitated. For both *Allosaurus fragilis* and *Allosaurus jimmadseni* the articulation with the ventral portion of the nasal is an overlap in which the frontals form a process to support the overlying nasal (Chure and Loewen 2020; Madsen 1976). This is a similar condition in *Acrocanthosaurus atokensis* (Eddy and Clarke 2011).

The frontals form a crescent shaped notch for the articulation with prefrontals. The dorsal contact with the postorbital is rounded laterally to meet the dorsal notch of the postorbital. Going dorsoventrally, the ventral contact with the postorbital is also rounded inward medially to meet the postorbital. The medial contact with the parietal is interdigitated and becomes less interdigitated laterally. The anterior medial surface of the interfrontal suture is straight anteriorly and becomes more interdigitated posteriorly.

Postorbitals

The postorbital makes up the dorsal margin of the laterotemporal fenestra and part of the lateral margin of the supratemporal fossa and fenestra. In lateral view, the postorbital contacts the squamosal and jugal. The ventral margin of the postorbital overlaps the dorsal portion of the jugal and tapers ventrally forming a lap joint. This ventral margin of the postorbital tapers into the orbital fenestra. This overlap is similar to that found in *Allosaurus jimmadseni* and *Acrocanthosaurus atokensis*, but differs in *Allosaurus europaeus* and *Ceratosaurus nasicornis* in which the ventral margin of the postorbital almost goes to the ventral margin of the orbital fenestra (Chure and Loewen 2020; Eddy and Clarke 2011; Madsen and Welles 2000; Mateus 2006). *Acrocanthosaurus atokensis* also has an intraorbital process of the postorbital, which occurs dorsally above the contact of the postorbital and jugal. The intraorbital process of the postorbital is not seen in CMP 279 or the *Allosaurus* genera. Continuing in lateral view, a groove in the squamosal supports the thin process of the postorbital ending close to the posterior margin of the squamosal. This is the same in *Allosaurus jimmadseni, Ceratosaurus nasicornis,* and *Acrocanthosaurus atokensis* (Chure and Loewen 2020; Eddy and Clarke 2011; Madsen and Welles 2000). In dorsal view, the postorbital contacts the frontal and parietal. The contact with the postorbital is similar to the contact with the frontal in which the parietal rounds inward medially to meet the postorbital.

Parietals

The parietal makes up the medial margins of the supratemporal fossa and fenestra. In anterior view the parietals curve dorsally before slightly curving anteriorly forming the parietal nuchal crest similar to that of *Allosaurus jimmadseni*, however in *Allosaurus jimmadseni* the parietal crest flares more anteriorly (Chure and Loewen 2020). In dorsal view, the parietal contacts the frontal, paroccipital, postorbital, squamosal, and supraoccipital. Continuing in dorsal view, the parietal nuchal crest curves ventrally where it eventually meets the squamosal. In posterior view, the parietal curves medially to meet the squamosal where it also rounds medially. At this contact the squamosal overlaps parietal similar to *Allosaurus jimmadseni* (Chure and Loewen 2020). The interparietal suture is interdigitated both on its anterior and posterior side.

Squamosals

The squamosal makes up part of the dorsal margin of the laterotemporal fenestra and the posterior margin of the supratemporal fossa and fenestra. In lateral view the squamosal contacts the postorbital, quadrate and quadratojugal similar to that of *Allosaurus jimmadseni* (Chure and Loewen 2020). The placement of the squamosal is also similar to *Allosaurus europaeus* and *Acrocanthosaurus atokensis* (Eddy and Clarke 2011; Mateus 2006). In dorsal view, the squamosal contacts the otoccipital in which the dorsal portion of the otoccipital forms a shelf to meet the posterior portion of the squamosal similar to *Allosaurus jimmadseni* (Chure and Loewen 2020).

Supraoccipital

The supraoccipital has an inverted T shape in posterior view but in dorsal view has triangular shape (Chure and Loewen 2020). The supraoccipital makes up about 2% of the dorsal margin of the foramen magnum. This is the same for all *Allosaurus fragilis* (Dino 2560) and is similar in placement to *Allosaurus jimmadseni* (Chure and Loewen 2020) This is not the case for *Ceratosaurus nasicornis* where the supraoccipital is 5 mm above the foramen magnum (Madsen and Welles 2000). In *Acrocanthosaurus atokensis* the supraoccipital is excluded from the foramen magnum, but posteriorly the supraoccipital make up only a small portion of the foramen magnum surface (Chure and Loewen 2020; Eddy and Clarke 2011).

In posterior view, the supraoccipital contacts the otoccipital and parietal. The parietal sits anterior

to the supraoccipital. At the dorsal end of the supraoccipital is the postnuchal sagittal crest that is a rounded knob that extends out posteriorly. The postnuchal sagittal crest sits ventrally to the tallest portion of the parietal nuchal crest. The dorsal surface of the postnuchal sagittal crest is notched. The postnuchal sagittal crest of the supraoccipital ventrally meets the dorsal margin of the paroccipital process. This contact extends laterally till it is overlapped by the parietal. The condition is similar in *Allosaurus jimmadseni* and *Acrocanthosaurus atokensis* (Chure and Loewen 2020; Eddy and Clarke 2011).

Otoccipital (Exoccipitals-Opisthotic)

The exoccipital and opisthotic are a fused set of bones in both *Allosaurus* genera and all dinosaurs in general (Sampson and Witmer 2007). This fused set of bones is known as the otoccipital and will henceforth be referred to as such. In posterior view, the otoccipital forms the lateral sides of the foramen magnum except for the dorsal margin which is occupied by the supraoccipital. This is similar to *Allosaurus jimmadseni* (Chure and Loewen 2020). The exoccipital portion of the otoccipital forms the dorsolateral surface of the occipital condyle. This is similar to *Allosaurus jimmadseni*, *Ceratosaurus nasicornis*, and *Acrocanthosaurus atokensis* (Chure and Loewen 2020; Eddy and Clarke 2011; Madsen and Welles 2000). Continuing in posterior view, the opisthotic portion of the otoccipital makes up the paroccipital process. The paroccipital process is a rectangular portion of the otoccipital that extends posterolaterally and deflects ventrally. The paroccipital process contacts the parietal, supraoccipital, basioccipital, basisphenoid, basal tubera, squamosal, and quadrate. The paroccipital process curves ventromedially to meet the quadrate and this contact slopes lateroventrally. This is similar to *Allosaurus jimmadseni* and *Acrocanthosaurus atonkensis* (Chure and Loewen 2020; Eddy and Clarke 2011).

Basioccipital

The basioccipital forms the ventral surface of the occipital condyle. In posterior view, the dorsal surface of the basioccipital is concave and contacts the medioventral portion of the otoccipital. The otoccipitals here are rounded dorsally, exaggerating the concavity of the basioccipital. This is similar for both *Allosaurus fragilis* (DINO 2560), and *Allosaurus jimmadseni* (MOR 696, DINO 11541) (Chure and Loewen 2020; Madsen 1976). The basioccipital is the ventral part of the foramen magnum, which only makes up a minor portion of the foramen magnum. This is similar to *Allosaurus jimmadseni* and *Acrocanthosaurus atokensis* (Chure and Loewen 2020; Eddy and Clarke 2011). In dorsal view the neck of the basioccipital is not constricted and the basioccipital is shield-shaped with the posterior margin being convex.

Jugals

The jugal has an inverted T shape and makes up the ventral margin of the orbital fenestra. The jugal also makes up part of the ventral margin of the laterotemporal fenestra. In lateral view, the jugal contacts the maxilla, postorbital, lacrimal, and quadratojugal. The jugal of CMP 279 deflects ventrally downwards which differs from the jugal of *Allosaurus jimmadseni* which is mostly straight possibly having a slight ventral downturn. This is one of the main characteristics used to distinguish between the two *Allosaurus* species in the Morrison Formation. The jugal of CMP 279 resembles that of other *Allosaurus fragilis* specimens (DINO 2560, USNM 4734) as well as *Allosaurus europaeus* (Mateus 2006). It differs from *Acrocanthosaurus atokensis* and *Ceratosaurus nasicornis* which both have relatively straight jugals like that of *Allosaurus jimmadseni* (Eddy and Clarke 2011; Madsen and Welles 2000). Continuing in lateral view, the jugal overlaps the maxilla as a small anterior process and makes up a very small ventral portion of the antorbital fossa. Dorsally above the jugal/maxilla contact the jugal rounds up dorsally to meet the lacrimal. The posterior end of the jugal forms a groove the accepts the process from the quadratojugal. Anteriorly in line with the process of the quadratojugal there are two large foramina. Internally these foramina branch into neurovascular canals, one of which goes dorsally through to the dorsal arm of the jugal and the other anteriorly through the to the maxilla. In medial view, the jugal contacts the ectopterygoid.

Quadratojugals

The quadratojugal has a backwards L shape and also makes up part of the ventral margin of the laterotemporal fenestra. In lateral view, the quadratojugals contact the squamosal, quadrate, and jugal. The dorsal margin of the quadratojugal overlaps the ramus of the squamosal. The quadratojugal completely overlaps the lateral margin of the quadrate except for the dorsal ramus of the quadrate. At this contact the quadratojugal articulates with the ventral edge of the quadrate's dorsal ramus. This placement is similar in all three *Allosaurus* genera, however, in both *Allosaurus fragilis* and *Allosaurus europaeus* the contact with the quadratojugal overlapping the squamosal ramus is flat (Madsen 1976; Mateus 2006). The contact where squamosal ramus overlaps the quadratojugal in *Allosaurus*

jimmadseni is convoluted (Chure and Loewen 2020). *Acrocanthosaurus atokensis* also appears to have a convoluted contact between the quadratojugal and squamosal ramus, but the anterodorsal edge of the quadratojugal is flat going from dorsoventrally (Eddy and Clarke 2011).

Quadrates

The quadrate is a bow shaped bone and one of the largest in the posterior portion of the skull. In lateral view the quadrate contacts the squamosal and quadratojugal. The ventral squamosal ramus overlaps the dorsal ramus of the quadrate. Continuing in lateral view the quadratojugal completely overlaps along the lateral surface of the quadrate. The only visible portion of the quadrate is its dorsal ramus posterior to the contact with the squamosal and quadratojugal. This is similar for all three *Allosaurus* genera; *Allosaurus fragilis*, *Allosaurus europeaus*, and *Allosaurus jimmadseni* (Chure and Loewen 2020; Madsen 1976; Mateus 2006). From the contact with the quadratojugal the quadrate curves medially to contact bones of the chondrocranium specifically the epipterygoid and basispheniod. In dorsal view, at the contact with the quadratojugal ventral to the paroccipital process is a large foramen known as the quadrate foramen.

The lateral and medial condyles on the ventral portion are similar in placement as *Allosaurus jimmadseni* (Chure and Loewen 2020). The lateral condyle fits into the cotylus of the articular and the medial condyle fits in the surangular/articular cotylus. The size of the quadrate is similar to *Allosaurus jimmadseni* in which it is short (Chure and Loewen 2020). This differs greatly to *Ceratosaurus nasicornis* in which the quadrate is tall and takes up a large portion of the laterotemporal fenestra in lateral view (Madsen and Welles 2000). A similar case can be seen in *Acrocanthosaurus atokensis* in which the quadrate is also tall (Eddy and Clarke 2011).

Ectopterygoids

The ectopterygoid is a U-shaped bone that bridges the outer cranium and palatine complex. In dorsal view the ectopterygoid curves out from the pterygoid laterally to meet the jugal. This curvature makes up the anterior margin of the suborbital fenestra. This notch, as noted by Ford (1997), likely stops the mandibles from proceeding more dorsally since the dorsal surangular perfectly fits within the notch. The surface that contacts the lateral surface of the pterygoid is longer both anteriorly and posteriorly than the surface that contacts the medial surface of the jugal, which overlaps the ectopterygoid. The ventromedial surface of the ectopterygoid has a pneumatic concavity that almost goes down to the ventral portion of the pterygoid. The ectopterygoid is similar to that both of *Allosaurus jimmadseni* and *Acrocanthosaurus atokensis* in shape and placement (Chure and Loewen 2020; Eddy and Clarke 2011). However, in *Acrocanthosaurus atokensis* the notch is longer and the pneumatic concavity on the medial surface is more recessed than that of CMP 279 (Eddy and Clarke 2011).

Pterygoids

The pterygoid is a long splint-like bone that makes up almost the entire length of the palate. Posteriorly in lateral view, the pterygoid contacts the bones of the chondrocranium specifically the basipterygoid, parasphenoid, and the epipterygoid. In lateral view, the pterygoid also contacts the dorsomedial edge of the quadrate. Continuing in lateral view, the pterygoid rises dorsally to meet the palatine. Plate 1 of the lateral view of the skull in Madsen (1976) does not include the remaining piece of the pterygoid. This piece of the pterygoid deflects dorsoventrally from the rest of the palatine that would articulate with the vomer. This is similar to *Allosaurus jimmadseni* but this differs from *Acrocanthosaurus atokensis* in which the vomer deflects dorsoventrally from the palatine rather than the pterygoid (Chure and Loewen 2020; Eddy and Clarke 2011). In medial view the anterior portion of the pterygoid contacts the maxilla on its medial surface. The posteroventral portion that is overlapped by the ectopterygoid has a pneumatic concavity as the pterygoid rounds ventrally.

Palatines

The palatine is a strut that supports the palatine complex. In lateral view, the palatine supports the pterygoid. The dorsal portion of the palatine is a thin splint that then expands and rounds out to overlap the pterygoid. In medial view, the medial surface of the maxilla overlaps the lateral surface of the palatine. This is similar to both *Allosaurus jimmadseni* and *Acrocanthosaurus atokensis* (Chure and Loewen 2020; Eddy and Clarke 2011).

Stapes

The stapes is not present in this specimen. This is a thin delicate bone and only appears in two *Allosaurus fragilis* specimens (UMNH 16605 and 16606) (Chure and Loewen 2020; Madsen 1976). The reasons the stapes is not present is unknown.

Vomers

The vomer is not present in this specimen. As previously mentioned, the vomer bones were most likely destroyed during the preparation process.

Laterosphenoids, Prootics, Epipterygoids, Basisphenoid, Parasphenoid, Basal Tubera,

Basipterygoid and Braincase

The chondrocranium and braincase of CMP 279 exhibits severe damage. These bones have been crushed and extensively restored, making it exceptionally challenging, if not nearly impossible, to differentiate between the chondrocranial elements and discern the precise shape of the braincase in the CT scans. Additionally, the skull of CMP 279 has been mounted in a manner that hinders research, as the posterior portions face a wall, rendering these bones mostly inaccessible. While some of these bones can be observed in lateral view through the laterotemporal fenestra, determining their exact placement is also complicated due to the extensive fractures and restoration. These bones appear to share similarities in placement with those found in both *Allosaurus fragilis* and *Allosaurus jimmadseni*; however, this assessment is made with limited confidence (Chure and Loewen 2020). Further investigation is needed, with a focus on conducting micro-CT scans on the braincase to precisely determine the placement of these bones.

Description of the Mandibles

Dentaries

The dentary is the largest and longest of the mandibular bones making the dentary the anterior one-half of the entire mandible (Madsen 1976). In dorsal view, the left dentary is straight until the anterior edge curves inward anteromedially to meet the right dentary. This compares with *Allosaurus fragilis* and *Acrocanthosaurus atokensis* (Eddy and Clarke 2011). This curvature differs from *Allosaurus jimmadseni* where there is little curvature on the anterior end of the dentary indicating a narrower snout than *Allosaurus fragilis* (Chure and Loewen 2020). However, the right dentary does not have the same anteromedially curvature on its anterior margin. Instead, the anterior edge has no curvature and slightly splays out laterally giving it a similar appearance to that of a dentary of *Ceratosaurus nasicornis* (Madsen and Welles 2000). This is most likely due to a pathology, which will be discussed further in the paper.

In anterior view, the lingual bar is thickest at its center bulging out medially, tapering dorsally towards the dental alveoli and supradentary. Underneath the lingual bar the meckelian groove is well developed. Beneath the meckelian groove the bone rounds out ventrally forming the bone's ventral margin. The first articulation with the splenial begins as a small process covering the meckelian groove. The mandibular symphysis occurs at the most anterior portion of the dentaries. The surface of the symphysis of both dentaries are flattened and well defined dorsoventrally. According to Madsen this would be a site of attachment for a ligament allowing for the kinetic movement between the two mandibles (Madsen 1976, 29). *Allosaurus fragilis* also has some of the highest gap angles among any theropod between 79°–90° based on a musculoskeletal constraint study (Lautenschlager 2015). The parastylic movement of the quadrate combined with the extension between the dentaries as well as other musculoskeletal constraints would permit the expansion of the gullet to swallow large pieces of food (Bakker 1998; McClelland 1990).

In medial view, the meckelian groove starts at the mandibular symphysis. The meckelian groove continues posteriorly from the symphysis until the anterior process of the splenial covers the meckelian groove becoming the meckelian foramen. This occurs on the posterior third of the dentary seen in *Allosaurus fragilis*. This placement compares with *Acrocanthosaurus atokensis and Allosaurus jimmadseni* (Chure and Loewen 2020; Eddy and Clarke 2011). In lateral view, there is a row of foramina that have an anteroposteriorly orientation parallel with the tooth row along the dentary's dorsolateral surface. Starting at the symphysis these anterior foramina are rounded. Going anteroposteriorly these foramina slightly shift ventrally and become larger as well as horizontally elliptical. This is also seen in *Allosaurus jimmadseni* (Chure and Loewen 2020). This differs from *Acrocanthosaurus atokensis* and *Ceratosaurus nasicornis* where the larger elliptical foramina are located in the lateral sulcus of the dentary (Eddy and Clarke 2011; Madsen and Welles 2000). On the anterior edge of the dentary, a few foramina run dorsoventrally parallel to the flattened surface of the symphysis and a row of foramina runs parallel to the ventral surface of the dentary. This is also present in *Allosaurus jimmadseni* (Chure and Loewen 2020). *Acrocanthosaurus atokensis* and *Ceratosaurus nasicornis* on the anterior ends do have foramina in this location but they are randomly oriented rather than being linear (Eddy and Clarke 2011; Madsen and Welles 2000).

Surangulars

The surangular is the second largest mandibular bone making up the posterior one-half of the mandible. In lateral view, the surangular contacts the dentary, angular, and articular. The posterior portion of the dentary overlaps the anterior portion of the surangular. This contact is sloped dorsoventrally until the surangular contacts the angular. Here the surangular is overlapped by the anterodorsal margin of the angular. Moving in a posterior direction the surangular makes up the dorsal margin of the external mandibular fenestra. Dorsally above the external mandibular fenestra is the anterior surangular

foramen. The anterior surangular foramen occurs ventral to the dorsal margin of the surangular and is a small round foramen. The anterior surangular foramen is connected to a neurovascular canal, which runs anteroposteriorly into the abductor fossa. The posterior surangular foramen occurs ventrally to a slightly rugose portion of the posterior surangular that slightly extends laterally. This is the lateral shelf surangular. The posterior surangular foramen goes through the surangular and exits into the abductor fossa. The position of both surangular foramen is similar for *Allosaurus fragilis*, *Allosaurus jimmadseni*, and *Acrocanthosaurus atokensis* (Chure and Loewen 2020; Eddy and Clarke 2011; Madsen 1976). Continuing in lateral view, the posterodorsal margin of the angular overlaps the angular process of the surangular posterior to the external mandibular fenestra. This contact goes anteroposteriorly until the angular becomes the posterior edge of the mandible.

In medial view, the surangular is overlapped by the prearticular, articular, and the antarticular. In dorsal view, the ramus of surangular extends medially and curves anteriorly to meet the posterior margin of the prearticular. Returning to medial view, the prearticular and surangular form the internal mandibular fenestra. The dorsomedial surface of the surangular is slightly rugose and extends medially. This is the medial self of the surangular. The medial and lateral shelf of the surangular is the attachment point for the *M. abductor mandibulae externus* (Sampson and Witmer 2007). The surangular, angular, coronoid, dentary, and prearticular form the abductor fossa. Overall, the surangular is similar to *Allosaurus fragilis* and *Allosaurus jimmadseni* (Chure and Loewen 2020; Madsen 1976).

Angulars

The angular is the third largest bone in the mandible and it is a plate-like bone that slightly bows out laterally forming the ventral portion of the mandible. In transverse view, the angular originates internally between the splenial and the dentary. Dorsal to the ventral margin of the splenial, the ramus of the angular has an upside-down comma-like shape. The ventral bulge of the comma rests on the splenial's lateral margin. The dorsal part of the comma curves and points laterally towards the medial edge of the dentary. Posteriorly, the angular switches position to the medial side of the dentary, increasing in size as the ventral margin of dentary tapers diagonally. This forms a lap or intermandibular joint where the dentary and splenial form the internal part of the abductor fossa (Chure and Loewen 2020; McClelland 1990). McClelland (1990) put forth that since there is no suturing between the dentary, splenial, and angular that this intermandibular joint was flexible in any direction, partly due to the angular ramus shape and placement. This would aid in the parastylic movement of the quadrate and dentary symphysial extension allowing for the enlargement of the gullet (McClelland 1990).

In lateral view, the dorsal margin of the angular forms the ventral edge of the external mandibular fenestra. Madsen (1976) illustrates the external mandibular fenestra of *Allosaurus fragilis* with a teardrop shape. This does not appear to be the case for *Allosaurus fragilis*, as CMP 279, DINO 2560 and USNM 4734 show an enlarged almond-shaped external mandibular fenestra. Chure and Loewen (2020) also illustrate this for *Allosaurus fragilis* and well as *Allosaurus jimmadseni.* In *Allosaurus jimmadseni* and *Acrocanthosaurus atokensis* however, the external mandibular fenestra is more anterior where the dentary forms a small portion of its ventral edge (Chure and Loewen 2020; Eddy and Clarke 2011). As Chure and Loewen (2020) have noted that Madsen (1976) showed the angular short of the "posterior limit of the mandible." In their analysis, they compared DINO 2560, USMN 4734 and BYU 9466, which all have an enlarged external mandibular fenestra similar to CMP 279 (Chure and Loewen 2020). This is not the case for *Acrocanthosaurus atokensis* where the surangular is the posterior margin of the mandible (Eddy and Clarke 2011).

Splenial

The splenial is a three-pointed plate-like bone. In medial view, the anterior portion of the splenial ends in a process, which covers the posterior portion Meckelian groove. Moving in a posterior direction the anterior mylohyoid foramen is along the splenial's anteroventral margin. The mylohyoid foramen is almost completely closed by small processes of the splenial with the ventral margin open. The ventral margin of the mylohyoid foramen would be closed by the splenial's articulation with the dentary. This is the condition for *Allosaurus fragilis* (Madsen 1976). For *Allosaurus jimmadseni*, the mylohyoid foramen is a notch with an open the ventral margin (Chure and Loewen 2020). In *Acrocanthosaurus atokensis* the splenial completely encloses the mylohyoid foramen (Eddy and Clarke 2011). Continuing in medial view, the posterior portion of the splenial is divided into two rami. The dorsal ramus is short having a boxy edge that overlaps the prearticular and coronoid. The ventral ramus is longer where it meets the ventral margin of the angular. The dorsal margin of the splenial overlaps both the supradentary and dentary.

Prearticulars

The prearticular is a lateromedially flattened bow or 'U' shaped bone forming the majority of the

medial edge of the abductor fossa. In medial view, the anterodorsal to anteroventral portion of prearticular is overlapped by the posterior edge of the splenial. Moving posteriorly the prearticular then overlaps the anterodorsal surface of the coronoid. On the anteroventral edge of the prearticular there is a notch called the posterior mylohyoid foramen, which Madsen (1976) called the intermandibular foramen. This is formed by the contact with the splenial and is an outlet for the anterior, medial, and posterior branches of the trigeminal nerve, this is also the case for *Allosaurus jimmadseni* (Chure and Loewen 2020; Schumacher 1973). On its posterior edge the prearticular overlaps the articular and makes up a small portion of the medial side of the glenoid fossa. This overlap however does not reach the most posterior edge of the articular. In transverse view, the prearticular bows out medially. The lateroventral edge of the prearticular contacts the medioventral surface of the angular which curves inward medially making a groove similar to *Allosaurus jimmadseni* (Chure and Loewen 2020). As noted in Chure and Loewen (2020), in lateral view the prearticular can be seen through the external mandibular fenestra for *Allosaurus* in general as well as *Acrocanthosaurus atokensis* (Eddy and Clarke 2011).

Articulars

The articular is a small rugose bone that makes up the articular surface for the quadrate. In lateral view the angular overlaps the articular on its ventral margin. The angular stops at the posterior margin of the articular making the angular the most posterior edge of the mandible. This is similar to that of *Allosaurus jimmadseni* and other more complete skulls of *Allosaurus fragilis* like DINO 2560 and USNM 4734 (Chure and Loewen 2020). However, this is not the case for *Acrocanthosaurus atokensis* where the angular does not reach the posterior limit of the mandible and does not reach the articular (Eddy and Clarke 2011). The surangular also overlaps the articular's most lateral surface making part of the articular surface. Here the surangular makes the lateral most part of the glenoid fossa. In dorsal view, the glenoid fossa is deep and slopes lateroventrally unlike the medioventral slope in *Allosaurus jimmadseni* (Chure and Loewen 2020). Proximal to the glenoid fossa is the foramen posterior chorda tympani which also slopes lateromedially. This is similar in *Allosaurus jimmadseni* but not in *Acrocanthosaurus atokensis* which slopes more mediodorsally giving it a slight upturned appearance (Chure and Loewen 2020; Eddy and Clarke 2011). The retroarticular process is proximal to the foramen posterior chorda tympani and forms the proximal wall of the chorda tympani. In medial view, the prearticular articulates the medial-most surface of the articular and is the most medial part of the foramen posterior chorda tympani. The contact here between the prearticular and articular also slopes lateroventrally similarly seen in *Allosaurus jimmadseni* (Chure and Loewen 2020). In *Acrocanthosaurus atokensis* the prearticular does not articulate with the articular (Eddy and Clarke 2011).

Supradentaries

The supradentary is a lateromedially flattened, thin, elongated, ovate, or almond shaped bone that runs most of the length of the dentary. In transverse view, the supradentary rests on the surfaces of the interdermal plates. In medial view, the supradentary begins at the third dental alveolus and continues the full length of the tooth row. The most posterior edge tapers after the last dental alveolus dorsally above the splenial. Between the ventral portion of the supradentary and dorsal margin of the lingual bar there is a dorsal secondary groove. This grove runs anteroposteriorly from the start of the supradentary to the dorsal surface of the where splenial articulates with the dentary.

Coronoids

The coronoid is also a lateromedially flattened triangular bone. The origin of the coronoid is unclear in the CT scans due to the internal fracturing, although it does appear to be a continuation of the supradentary, which is a similar condition in *Acrocanthosaurus atokensis* (Eddy and Clarke 2011). The supradentary continues anteroposteriorly between the dentary and splenial first, then the dentary and prearticular. This is also seen in *Allosaurus jimmadseni* where, "the posteroventral margin is overlapped by the splenial" (Chure and Loewen 2020). In Madsen (1976) and Chure and Loewen (2020) both describe the coronoid and supradentary as separate bones. Personal observations were made of individual specimens in both studies. Without the aid of CT scans, it is highly unlikely that these personal observations would observe the internal structures of these bones. It is also likely that the sutures that appear to be a continuation of the supradentary could be artifacts of the internal fracturing, but this seems unlikely since a related species (*Acrocanthosaurus atokensis)* has similar bone placement (Eddy and Clarke 2011). If this is the case, then this is not two distinct separate bones and should possibly be renamed or clarified in future literature about the true nature of the supradentary and coronoid in different theropod species.

In transverse view, internally the coronoid anteroposteriorly continues between the surangular and splenial before eventually being overlapped by the anterior portion of the prearticular. The

coronoid curves inward medially forming a sulcus above the dorsal margin of the anterior portion of the prearticular. Dorsally above the coronoid the surangular also curves in medially to form another sulcus. In medial view, the coronoid erupts from the overlapping anterior portion of the prearticular. The posterior margin of the coronoid forms the dorsal edge of the abductor fossa along with the surangular.

Antarticulars

The antarticular is a small pyramidal shaped bone off the posteroventral edge of the prearticular. In medial view, the antarticular forms a pocket with the prearticular, surangular, and angular as in *Allosaurus jimmadseni* (Chure and Loewen 2020). In *Acrocanthosaurus atokensis* an ossified antarticular is nonexistent and only appears to be present in *Allosaurus* and possibly the tyrannosauroid *Bagaraatan ostromi* (Chure and Loewen 2020; Eddy and Clarke 2011; Osmolska 1996). Chure and Loewen (2020) point out that the only in situ preservation of the antarticular is found in complete skulls like DINO 2560 and MOR 693. This is also the case for CMP 279 where both antarticulars are present. Due to its small nature and possible loose connection to the prearticular this bone is likely to be transported away from the skull during deposition (Chure and Loewen 2020). This is evident in the skull of DINO 11541 and the disarticulated *Allosaurus fragilis* from Cleveland-Lloyd Quarry, since the antarticular is an isolated element not associated with any other jaw material (Chure and Loewen 2020; Madsen 1976).

Description of the Ceratobranchials

The hyoid is a slightly bow-shaped bone. Both the left and the right hyoid are present in CMP 279 (figs. 19 and 20). The position found during the excavation is currently unknown. Both hyoids have breakage near the anterior end of the bones, but the right hyoid has additional breakage at mid-length causing it to be dorsally upturned. In lateral view, the anterior portion of the hyoid is lateromedially flattened and smooth. It extends more dorsally and ventrally than the posterior portion. The posterior portion is also lateromedially flattened ending in smaller rounded point. In dorsal view, the bone becomes more rod like slightly curving laterally moving anteroposteriorly. Hyoids in theropod dinosaurs are seldom preserved and the only recorded example of *Allosaurus fragilis* hyoids belong to USNM 4734 (Carrano, Loewen, and Evers 2018; Chure and Loewen 2020). The right and left hyoids were originally labeled as cervical ribs and are probably missing the anterior tips (Carrano, Loewen, and Evers 2018). There are no further descriptions of the hyoids of USNM 4734, which make it difficult to compare with the hyoids of CMP 279. Carrano, Loewen, and Evers (2018) and Chure and Loewen (2020) both report that the hyoids of DINO 11541an *Allosaurus jimmadseni* specimen are identical to those of USNM 4734. It appears that there is no difference between the hyoids of the two North American *Allosaurus* genera (*Allosaurus fragilis* and *Allosaurus jimmadseni*). The hyoids of CMP 279 compare with those of *Allosaurus jimmadseni* (DINO 11541).

Fig. 19. (A) Lateral view of the left hyoid. (B) Medial view of the left hyoid. The scale bar is 10 cm.

Fig. 20. (A) Lateral view of the right hyoid. (B) Medial view of the right hyoid. The scale bar is 10 cm.

Dentition

General Dentition Description

The teeth of CMP 279 match teeth found in *Allosaurus fragilis* and has a total of 74 dental alveoli, which would be in the tooth count range of 66–78 matching *Allosaurus fragilis* (Madsen 1976). The teeth have a general backwards D shape in lateral view. In dorsal view, the apical of the teeth have a lenticular cross-section which grades into an oval cross-section near the cervix and then grades into a figure-eight cross-section at the root. The labial and lingual surface is smooth. The mesial and distal carinas both have denticles. The denticles are rounded and an individual denticle is less than a millimeter in size (fig. 21). The anterior teeth are relatively straight

Fig. 21. Zoomed in view of the teeth in the left dentary showing the rounded denticles on the surface of the distal carina.

moving posteriorly the teeth increasingly become more recurve. The posterior teeth have the most recurve. This is the same for both the premaxilla/maxillary dentition and the dentary dentition. The terminology used for this dentition description is adapted from Hendrickx, Mateus, and Araùjo (2015).

Dentary Dentition

Madsen (1976) observed between fifteen to seventeen dental alveoli in the dentary. In CMP 279 there are seventeen alveoli in both the right and left dentary. This differs from *Allosaurus jimmadseni* in which it has the highest tooth count among other allosauroids with nineteen alveoli (Chure and Loewen 2020). *Acrocanthosaurus atokensis* has seventeen alveoli and *Ceratosaurus nasicornis* has 11 alveoli possibly 12 (Eddy and Clarke 2011; Madsen and Welles 2000). The right dentary has 14 exposed teeth in various states of eruption. Nine of the teeth are fully erupted including two that are broken missing the tips of the crowns. Three of the teeth are not fully erupted with only the tips of the crowns visible. The rest of the teeth were either shed by the animal in life or shed during the taphonomic and/or depositional processes. With the use of the CT scans germ teeth can be seen in various positions of replacement (fig. 22). Several of the germ teeth are intact showing only one germ tooth in the replacement position. There are several examples of two germ teeth in replacement. Most of the germ teeth are crushed on the anterior and posterior portions of the dentary. The left dentary has 11 exposed teeth in various states of eruption. Six of the teeth are fully erupted with four that are not fully erupted exposing only the tips of the crowns. The germ teeth in the left dentary are crushed and it is unclear how many germ teeth are present.

Premaxillary Dentition

Madsen (1976) observed that there are five alveoli in the premaxilla and there was not any variation in that amount for *Allosaurus fragilis*. In both the right and left premaxilla of CMP 279 there are five alveoli which differs from *Acrocanthosaurus atokensis* that has four alveoli in the premaxilla (Eddy and Clarke 2011). The presence of five alveoli in the premaxilla appears to be true amongst *Allosaurus* including *Allosaurus jimmadseni* but it is uncertain whether *Allosaurus europaeus* is similar since the premaxilla was not discovered (Eddy and Clarke 2011; Mateus 2006). In the right premaxilla all five teeth are fully erupted. In the left premaxilla four of the teeth are fully erupted with the fourth tooth missing. Germ teeth are mostly intact with one germ tooth in replacement for each tooth (fig. 23). Few of the germ teeth are completely crushed.

Maxillary Dentition

Madsen (1976) observed that the number of dental alveoli varies in *Allosaurus fragilis* between 14 to 17 alveoli. Out of the 37 maxilla he observed, the majority had 16. In the right and left maxilla of CMP 279, 15 dental alveoli were observed. In *Allosaurus jimmadseni* the number of maxillary teeth is 14, whereas there are 12 in *Acrocanthosaurus atokensis* and ten in *Ceratosaurus nasicornis* (Chure and Loewen 2020; Eddy and Clarke 2011; Madsen and Welles 2000). There are nine teeth that are fully erupted and two that are partially erupted in the right maxilla. In the left maxilla there are six fully erupted teeth, two partially teeth erupted and one that is partially broken at the maxilla/premaxilla suture. Germ teeth are mostly intact with one germ tooth in replacement for each tooth (fig. 24). Few of the germ teeth are completely crushed.

Discussion

Neurovascular Canals

The use of CT scans has revealed some interesting aspects of *Allosaurus fragilis* anatomy and possible behavior. Trigeminal foramina in CMP 279 occur

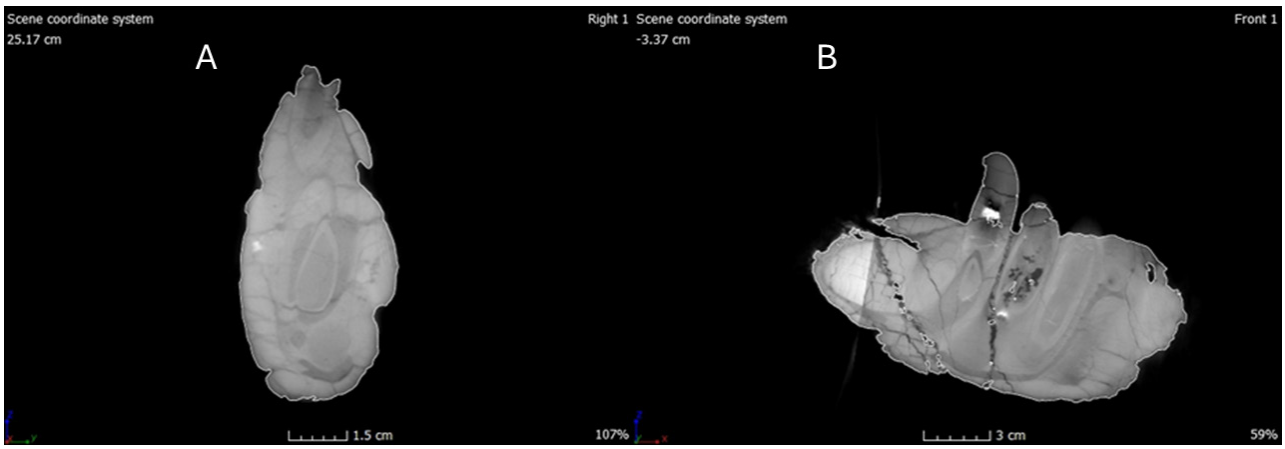

Fig. 22. (A) A single CT slice from the right dentary in internal frontal view showing a single germ tooth. (B) A single CT slice from the right dentary in internal medial view showing a two germ teeth inside already erupted tooth.

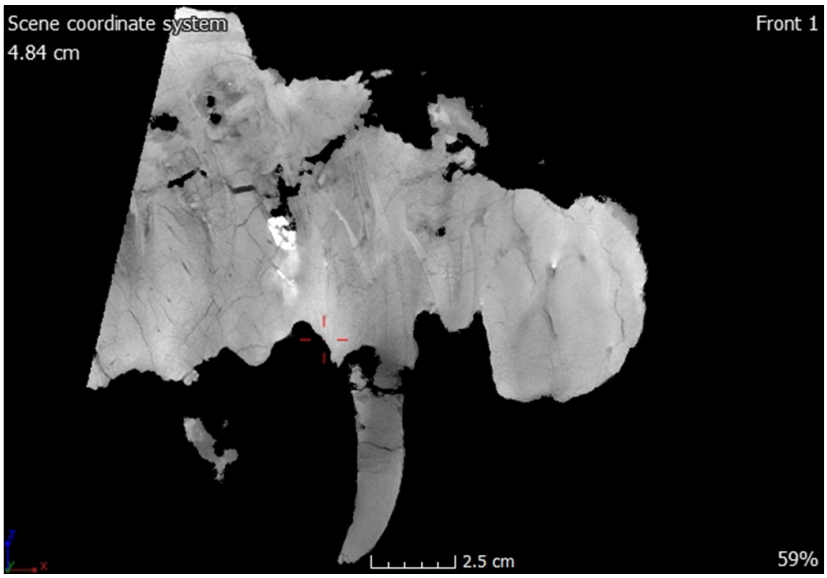

Fig. 23. A single CT slice from the left premaxilla in internal medial view showing a single germ tooth inside an already erupted tooth.

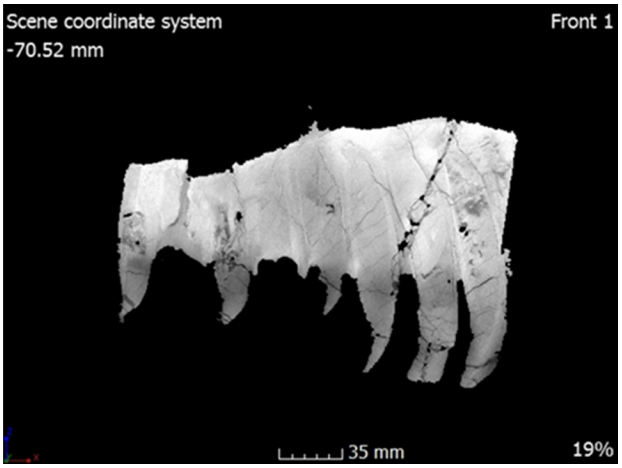

Fig. 24. A single CT slice from the left maxilla in internal medial view showing the internal tooth structure with a single germ tooth inside an already erupted tooth.

in other *Allosaurus fragilis* specimens like DINO 2560 and USNM 4734. Trigeminal foramina are also present in *Allosaurus* jimmadseni specimens like DINO 11541, MOR 693 and SMA 0005. The trigeminal foramina in CMP 279 in the dentary, premaxilla, maxilla, and jugal most likely represent outlets for blood vessels and nerves separate from the other vascularization of the skull (fig. 25). The trigeminal foramina in the dentary connects to internal anastomosing neurovascular canals exiting into the adductor fossa and probably represents connection to the mandibular branch of the trigeminal nerve (figs. 26 and 27). The trigeminal foramina in the premaxilla, maxilla and jugal connect to a network of neurovascular canals that run most of the length of the skull and probably represent the connection to the trigeminal nerve (figs. 28–30). Foramina connecting to neurovascular canals has been observed in several theropod species *Neovenator salerii, Spinosaurus aegyptiacus*, *Tyrannosaurus rex*, *Majungosaurus crenatissimus*, *Daspletosaurus horneri,* and *Skorpiovenator bustingorryi* (Barker et al. 2017; Bouabdellah, Lessner, and Benoit 2022; Carr et al. 2017; Cerroni et al. 2022; Dal Sasso, Maganuco, and Cioffi 2009; Ibrahim et al. 2014; Porter and Witmer 2020). Some marine reptiles have also been observed to possess foramina connecting to neurovascular canals, an ichthyosaur *Protoichthyosaurus prottaxalis*, a plesiosaur *Marcoplata tenuiceps*, a mosasaur *Taniwhasaurus antarticus* and the pliosaur *Pliosaurus kevani* (Álvarez–Herrera, Agnolin, and Novas 2020; Foffa, et al. 2014; Ketchum and Smith 2010; Lomax, Porro, and Larkin 2019). Neurovascular canals and trigeminal foramina have been extensively researched in extant crocodilians and certain birds. For both crocodilians and birds, these foramina function as conduits for nervous and vascular organs acting as a multifunctional external integumentary sensory organ. These functions include mechcanoreception for detecting food, thermosensors for detecting nest temperature or heat exchange, and as chemosensors (Barker et al. 2017).

Fig. 25. Foramina on the lateral side of the right dentary. The scale bar is 1 cm.

The function of these neurovascular canals and trigeminal foramina in large theropods is difficult

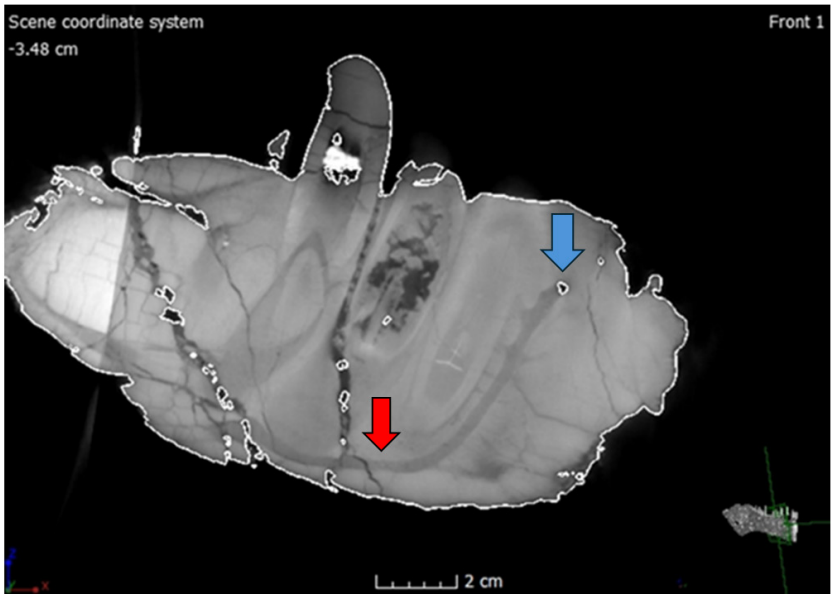

Fig. 26. A single CT slice in internal lateral view from the right dentary showing a single foramen (highlighted by the blue arrow) connected to neurovascular canal (highlighted by the red arrow).

Fig. 27. A single CT slice in internal frontal view from the right dentary showing multiple neurovascular canals highlighted by the blue arrows.

to determine since current extant taxa are smaller in size and inhabit different ecological niches, with *Spinosaurus aegyptiacus* possibly being an exception (Barker et al. 2017; Ibrahim et al. 2014). A study conducted on a *Spinosaurus aegyptiacus* rostrum using CT scans determined that the trigeminal foramina in the premaxilla were used as pressure receptors that were connected to the trigeminal nerve similar to that of extant crocodilians (Dal Sasso, Maganuco, and Cioffi 2009). Also, an oxygen isotope study determined the *Spinosaurus aegyptiacus* was inhabiting similar niches as those of modern crocodilians and turtles thus having a semiaquatic lifestyle (Amiot et al. 2010). It has been observed that crocodilians have large trigeminal foramina correlating to their semiaquatic lifestyle and the increased use of somatosensory capabilities (Leitch and Catania 2012). Scaling analyses of the trigeminal foramina determined that non-avian theropods like *Allosaurus* have smaller foramina compared to crocodilians (Lessner et al. 2023). The smaller trigeminal foramina in large theropods like *Allosaurus* may correlate more with a terrestrial lifestyle (Lessner et al. 2023). The functionality of these foramina probably indicates that *Allosaurus* had some facial sensitivity. As to what behaviors were

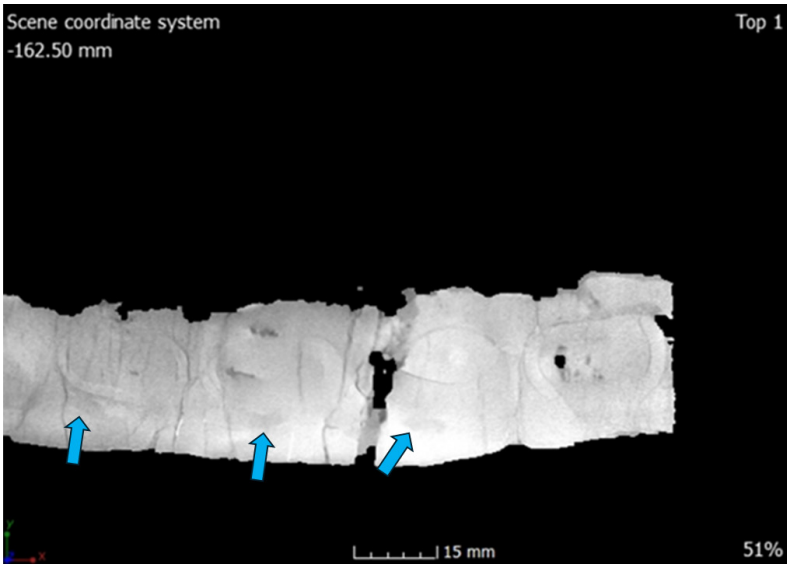

Fig. 28. A single CT slice in ventral view from the left maxilla showing neurovascular canals highlighted by the blue arrows.

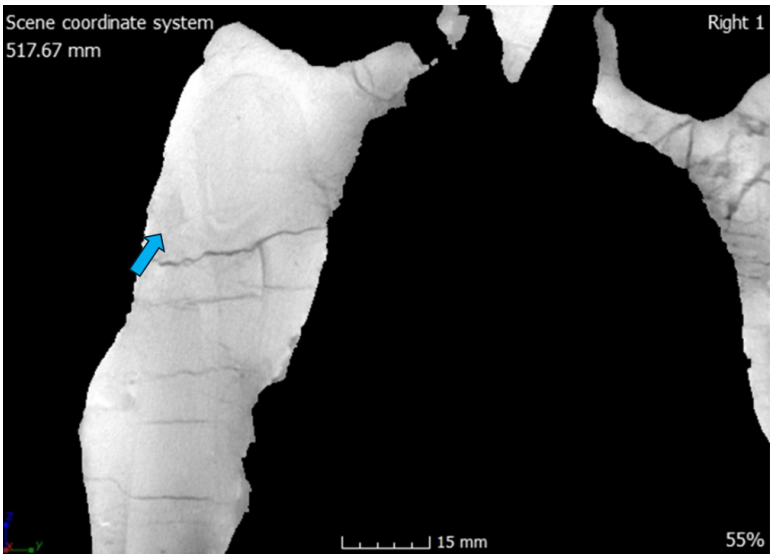

Fig. 29. A single CT slice in internal posterior view from the left premaxilla showing a single neurovascular canal highlighted by the blue arrow.

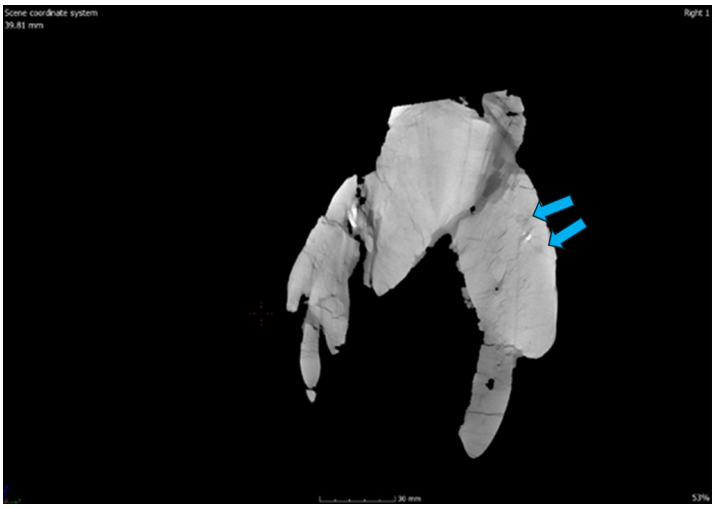

Fig. 30. A single CT slice in internal posterior view from the right premaxilla showing two neurovascular canals highlighted by the blue arrows.

used, this is difficult to determine without direct fossil evidence. For therapods this facial sensitivity has been hypothesized to be used for nesting behaviors such as testing nest temperature, social interactions such as facial biting, or feeding behaviors used during defleshing (Barker et al. 2017; Bouabdellah, Lessner, and Benoit 2022). These foramina could also possibly indicate the presence of a keratinous rhamphotheca lip-like or cheek-like extensions (Barker et al. 2017; Bouabdellah, Lessner, and Benoit 2022).

Possible Pathologies

There appears to be several possible pathologies found on both mandibles, more specifically the right and left surangular, and the right dentary. There is also another possible pathology on the right lacrimal. The pathology on the right dentary occurs at its most anterior portion on the dorsolateral surface at tooth 1 and 2 (fig. 31). When viewing the CT scans, there is abnormal bone growth around the boundary of tooth 1 and 2, which might indicate an abscess due to osteomyelitis (fig. 32). Bone thickening around the infected area is a common identifier in osteomyelitis (Hamm et al. 2020; Reisz et al. 2011). There needs to be more research done to accurately determine if this is a case of osteomyelitis or if it is related to the second aspect of the dentary pathology. The second pathology on the right dentary is that the anterior portion is laterally outturned. This appears to be separate from the possible abscess as evidenced from the teeth. The first and second tooth have grown close together near the medial symphysis. This growth appears to have caused the second tooth to swell and the posterior surface of the first tooth to become flattened (fig. 33). The outturned portion has also caused damage to the surrounding foramina in which several of the foramina openings are enlarged (fig. 34).

Pathologies on the dentaries of *Allosaurus* appear to be rare compared to pathologies throughout the rest of the skeleton (Madsen 1976). However, there are two examples of dentary pathologies USNM 2315 and SMA 0005. USNM 2315 is assigned to the species *Labrosaurus ferox* and is an isolated left dentary. Many have assumed that the dentary belongs to *Allosaurus fragilis* since its proportions and shape match the species (Madsen and Welles 2000). The pathology is a 'U' shaped notch out of the anterodorsal surface. Gilmore (1920) thought the notch might be due to an injury but did not make a definite conclusion since the dentary lacked any deformities that would indicate an injury. Madsen and Welles (2000) concluded that this was indeed a pathology but noted that the posterior one third of the pathology is exaggerated by overpreparation and distortion postmortem. Other researchers have considered the notch to be completely natural (Madsen and Welles 2000). According to Tank and Currie (1998) the notch appears to be a bite mark that was heavily remodeled during the healing process.

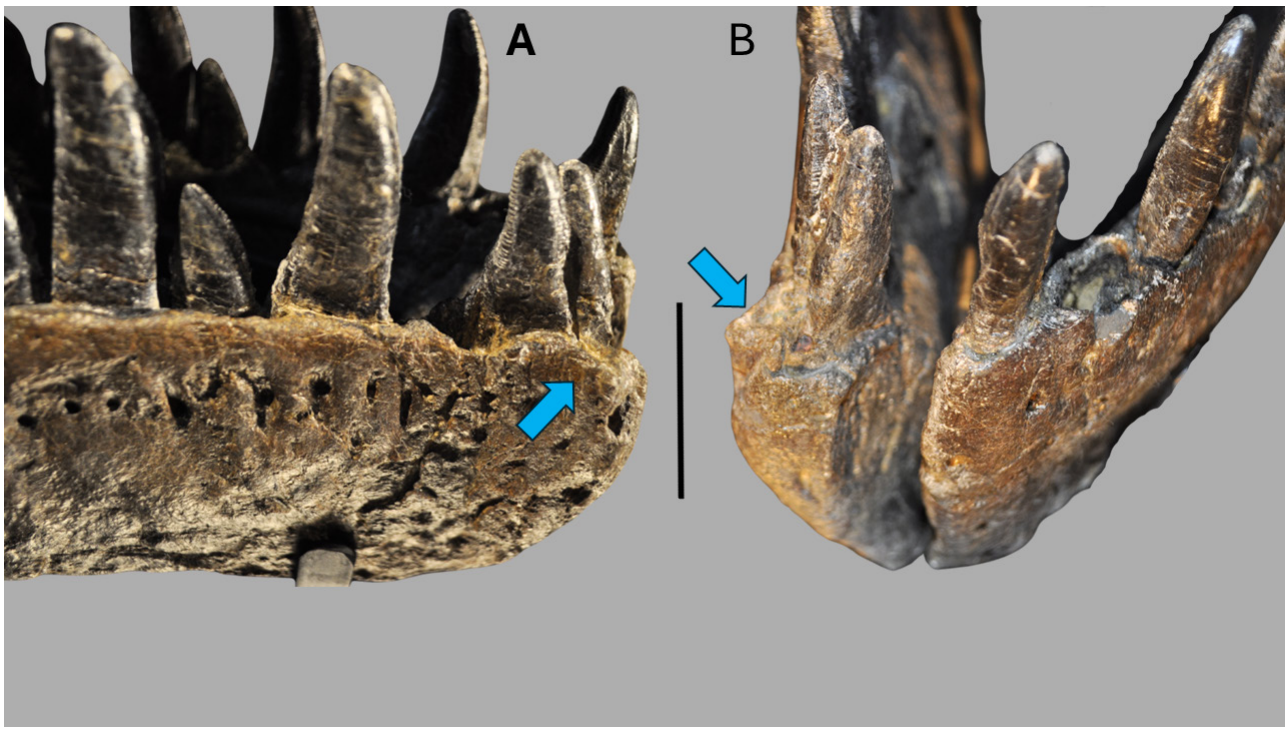

Fig. 31. (A) Right lateral view of the right dentary showing the abnormal bone growth around tooth 1 and 2. (B) A frontal view of the right dentary showing the same abnormal bone growth. Both are highlighted by the blue arrows. The scale bar is 5 cm.

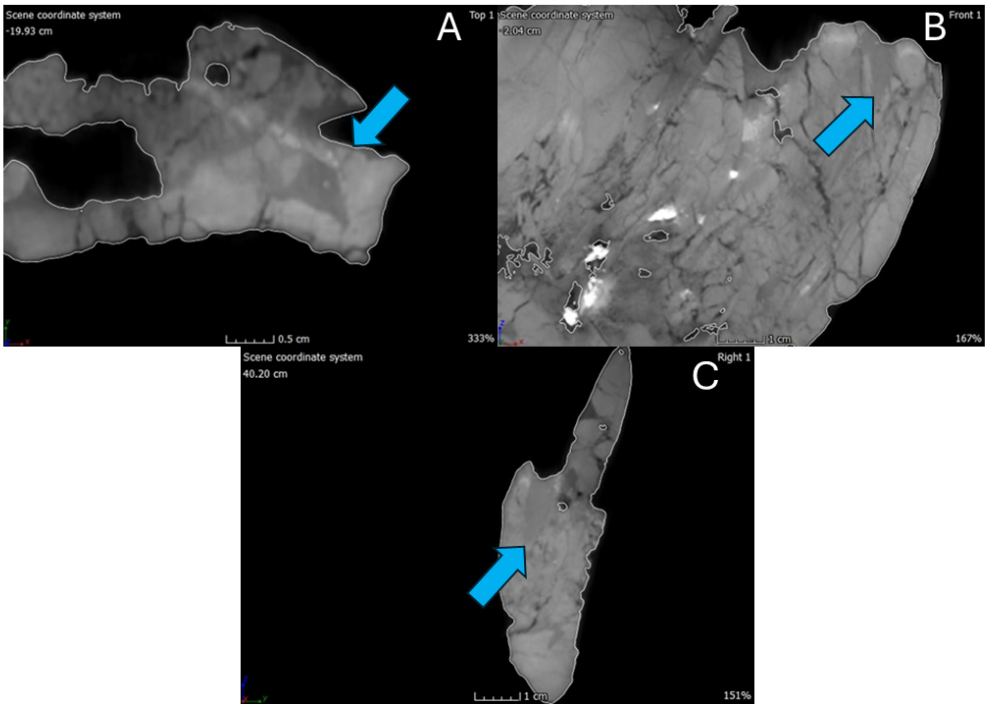

Fig. 32. (A) A single CT slice from the right dentary of the possible abscess in dorsal view. (B) A single CT slice from the right dentary of the possible abscess in internal lateral view. (C) A single CT slice from the right dentary of the possible abscess in anterior view.

SMA 0005 a specimen of *Allosaurus jimmadseni* has a pathology on the anterior portion of the left dentary where the anterior portion curves ventrally giving it the shape reminiscent of Spinosaurid dinosaurs. Foth et al. (2015) concluded that the pathology of SMA 0005 is most likely due to either facial biting or possibly the result of a developmental malformation during the individual's ontogeny. This analysis included a comparison USNM 2315 among others (Foth et al. 2015). It is possible that pathology on the right dentary of CMP 279 is a result of either facial biting hypothesized for other large theropods or a malformation occurring during the animal's development (Foth et al. 2015; Tanke and Currie 1998).

Two other possible pathologies occur on the right and left surangulars. In lateral view, the right surangular has a pit mark near the dorsal margin of the external mandibular fenestra (fig. 35). This pit mark is shallow but is slightly deeper on the anterior side where there appears to be bone growth. It is uncertain to what this pathology represents since it does not match any known facial pathologies known for theropods in general and *Allosaurus*. This

Fig. 33. The right dentary in anterior view showing the growth pattern of teeth 1 and 2 and outturned nature of the dentary. Also refer to fig. 31 for a comparison of the abnormal tooth growth. The scale bar is 5 cm.

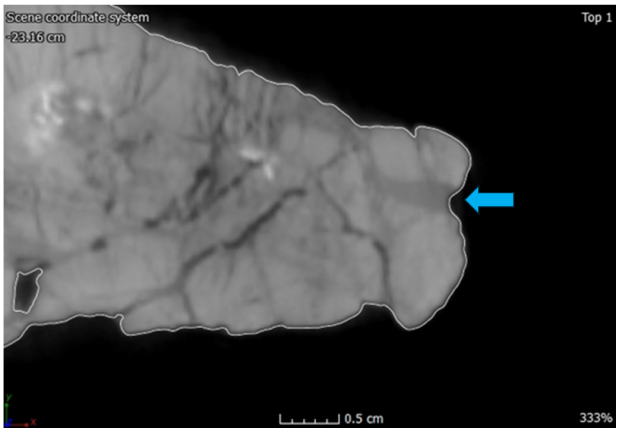

Fig. 34. A single CT slice of the right dentary in dorsal view showing the enlarged foramen highlighted by the blue arrow. Also refer to figs. 25, 31, and 33 for comparison of the size of the foramen along the right dentary.

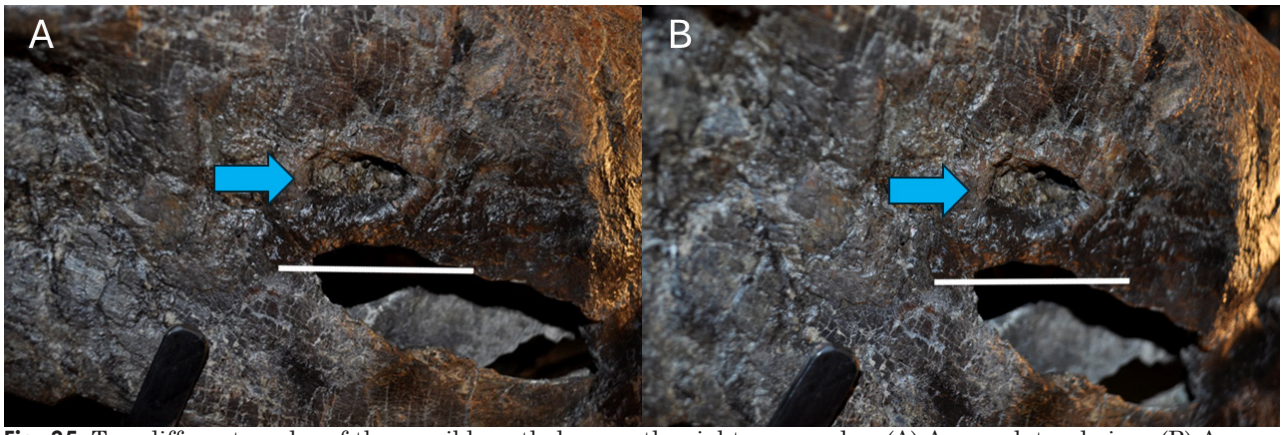

Fig. 35. Two different angles of the possible pathology on the right surangular. (A) A more lateral view. (B) A more posterior view. Both are highlighted by the blue arrows. The scale bar is 5 cm.

pathology most likely occurred before the animal's death since there is remodeled bone around the pit mark. In lateral view of the left surangular near the dorsal margin of the angular there is a piece of the missing surangular (fig. 36). The missing piece of bone is rectangular in shape and is diagonally orientated. The final possible pathology is a small circular hole on the dorsal surface of the right lacrimal crest (fig. 37). It is uncertain what these pathologies on the left suranglar and right lacrimal represent. Both could be examples of facial biting, or something that occurred during deposition since there is no additional bone growth surrounding either orifice. For at least these two possible pathologies (left surangular and right lacrimal), another possible explanation is these are a result of over preparation, which is the most likely reason for certain missing skull elements; the vomers and possibly the stapes.

Fig. 36. The possible pathology on the left surangular is highlighted by the blue arrow. The scale bar is 5 cm.

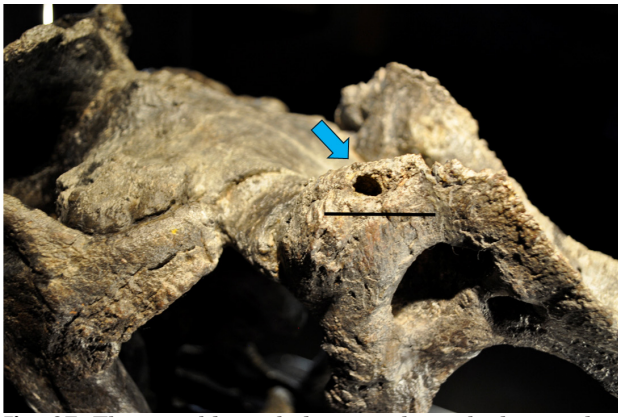

Fig. 37. The possible pathology on the right lacrimal is highlighted by the blue arrow. The scale bar is 5 cm.

Conclusion

CMP 279 is identified as belonging to the species *Allosaurus fragilis*, and it shares several distinctive characteristics with the neotype (USNM 4734) and paratype (DINO 2560) of this species. These key features include the ventral margin of the jugal, which deflects ventrally at mid-length, the presence of large lacrimal horns, two significant pneumatic openings that open laterally near the cornual process, the tooth count between 66 and 78, and the nasal structure, which lacks significant rugosity, indicating the absence of a large bilateral crest. These distinguishing features not only classify CMP 279 as *Allosaurus fragilis* but also differentiate it from other theropods in the Jurassic Morrison Formation.

Our utilization of CT scans allowed for more precise determination of sutures, surpassing what traditional observations of cranial anatomy could provide. Furthermore, these scans unveiled the first documented presence of neurovascular canals and a potential case of osteomyelitis in a dentary of *Allosaurus fragilis*. The pathologies observed in the skull require further investigation to understand their origins and to identify any potential pathologies in the rest of the skeleton.

Future research on CMP 279 should encompass a detailed description of the axial and appendicular skeletal material, as well as a more comprehensive examination of dental microwear. Additionally, there is an opportunity for research to ascertain the purpose of the foramina in terrestrial theropods, specifically *Allosaurus fragilis*. Additionally sedimentological and taphonomic studies of the CMP 279 site would

provide a more comprehensive understanding of the deposition of the skeleton during the Flood.

In conclusion, the skull of CMP 279 has offered valuable insights into the species *Allosaurus fragilis*, and further research promises to yield even more valuable information.

Institution Abbreviations

BYU. Earth Science Museum, Brigham Young University, Provo, Utah, United States of America.
CMP. Creation Museum, Petersburg, Kentucky, United States of America.
DINO. Dinosaur National Monument, Jensen, Utah, United States of America.
IFPUB. Institut für Geologische Wissenschaften der Freie Universitat, Berlin, Germany.
ML. Museu da Lourinha, Lourinha, Portugal.
MOR. Museum of the Rockies, Bozeman, Montana, United States of America.
SMA. Sauriermuseum of Aathal, Aathal, Switzerland.
USNM. National Museum of Natural History, Smithsonian Institution, Washington D.C., United States of America.
UMNH VP. Natural History Museum of Utah (Formerly the University of Utah of Natural History and previous catalogued under UUVP) Salt Lake City, Utah, United States of America.
YPM. Yale Peabody Museum, New Haven Connecticut, United States of America.

Authors' Statement

We, the authors, are independent researchers with no affiliations to Answers in Genesis. Nevertheless, we would like to express our gratitude to those who generously contributed to AiG, enabling this research to take place. We appreciate the opportunity to be involved in this research and want to inform fellow researchers that CMP 279 is open for study by all interested parties regardless of their perspectives on creation or evolution. This includes access to the scans and any skeletal material. For further inquiries regarding CMP 279, please feel free to contact the head of research at AiG, Dr. Georgia Purdom or Dr. Gabriela Haynes, paleontologist at AiG.

Acknowledgements

We wish to extend our sincere gratitude to Dr. Andrew Snelling and Dr. Gabriela Haynes of Answers in Genesis for their invaluable support in facilitating our research and for making all project-related files readily accessible. We also appreciate their patience, as this project extended beyond its initial timeline, as is often the case in scientific research.

Special thanks are also due to James Berger from 3D Engineering Solutions for his remarkable work in conducting the scans and his invaluable assistance in resolving software-related challenges. We extend our appreciation to Matt Petrone, who generously provided access to his photographs of several specimens, including MOR 693, DINO 2560, and CMP 279.

We are deeply thankful to the reviewers whose constructive critiques and comments significantly contributed to improving this publication. We would like to acknowledge the valuable insights and support provided by Dr. John Whitmore and Thomas Rice of Cedarville University, who offered their expertise and provided access to laboratory equipment.

Lastly, Nicholas Rush would like to express his appreciation to his wife, who was a tremendous help in editing this paper and spent hours working to clean up the citations.

Dedication

While we conducted this research, we learned the unfortunate news of Joe Taylor's passing. We are saddened by his loss and want to recognize one of his many contributions to young age creationism. We understand the skull has a tumultuous history, but we believe Joe Taylor does not receive the recognition that he deserves. His efforts and knowledge lead to the excavation and preservation of an exquisite Allosaurus skull. It is for these reasons that we dedicate this work to Joe Taylor. We hope that his contributions, especially those in paleontology and the skull of CMP 279 continue to inspire the next generation of young age creationists.

References

Aaron, M. 2014. "Discerning Tyrants from Usurpers: A Statistical Baraminological Analysis of Tyrannosauroidea Yielding the First Dinosaur Holobaramin." *Answers Research Journal* 7 (November 26): 463–481. https://answersresearchjournal.org/first-dinosaur-holobaramin/.

Álvarez–Herrera, Gerardo, Federico Agnolin, and Fernando Novas. 2020. "A Rostral Neurovascular System in the Mosasaur *Taniwhasaurus antarcticus*." *The Science of Nature— Naturwissenschaften* 107, no. 3 (June): 1–5.

Amiot, Romain, Eric Buffetaut, Christophe Lécuyer, Xu Wang, Larbi Boudad, Zhongli Ding, François Fourel, et al. 2010. "Oxygen Isotope Evidence for Semi-Aquatic Habits Among Spinosaurid Theropods." *Geology* 38, no. 2 (February): 139–142.

Anderson, Calvin, et al. 2014. *Sedimentology and Stratigraphy Class*. Unpublished Field Notes.

Bakker, Robert T. 1998. "Brontosaur Killers: Late Jurassic Allosaurids as Sabre-Tooth Cat Analogues." *GAIA: Revista de Geociências* 15 (December): 145–158.

Barker, Chris Tijani, Darren Naish, Elis Newham, Orestis L. Katsamenis, and Gareth Dyke. 2017. "Complex Neuroanatomy in the Rostrum of the Isle of Wight theropod *Neovenator salerii*." *Scientific Reports* 7, no. 1 (16 June): 3749.

Bouabdellah, Florian, Emily Lessner, and Julien Benoit. 2022. "The Rostral Neurovascular System of *Tyrannosaurus rex*." *Palaeontologia Electronica* 25, no. 1 (January): 1–20.

Carpenter, Kenneth. 2010. "Variation in a Population of Theropoda (Dinosauria): *Allosaurus* from the Cleveland-Lloyd Quarry (Upper Jurassic), Utah, USA." *Paleontological Research* (BioOne) 14, no. 4 (December): 250–259.

Carr, Thomas D., David J. Varricchio, Jayc C. Sedlmayr, Eric M. Roberts, and Jason R Moore. 2017. "A New Tyrannosaur with Evidence for Anagenesis and Crocodile-like Facial Sensory System." *Scientific Reports* 7, no. 1 (30 March): 44942.

Carrano, Matthew T., Mark A. Loewen, and Serjoscha W. Evers. 2018. "Comment (Case 3506)—Conservation of *Allosaurus* Marsh, 1877 (Dinosauria, Theropoda): Additional Data in Support of the Proposed Neotype for its Type Species *Allosaurus fragilis* Marsh, 1877." *The Bulletin of Zoological Nomenclature* 75, no. 1 (31 May): 59–64.

Cerroni, Mauricio A., Juan I. Canale, Fernando E. Novas, and Ariana Paulina-Carabajal. 2022. "An Exceptional Neurovascular System in Abelisaurid Theropod Skull: New Evidence from *Skorpiovenator bustingorryi*." *Journal of Anatomy* 240, no. 4 (22 June): 612–626.

Chure, Daniel, and Mark Loewen. 2020. "Cranial Anatomy of *Allosaurus jimmadseni*, a New Species from the Lower Part of the Morrison Formation (Upper Jurassic) of Western North America." *PeerJ* 8 (January 24): e7803. https://doi.org/10.7717/peerj.7803.

Dal Sasso, Cristiano, Simone Maganuco, and Armando Cioffi. 2009. "A Neurovascular Cavity Within the Snout of the Predatory Dinosaur Spinosaurus." In *First International Congress on North African Palaeontology, Program and Abstract Volume*. Edited by N.-E. Jalil, 30–31. Marrakech, Morocco: Cadi Ayyad University.

Eddy, Drew R., and Julia A. Clarke. 2011. "New Information on the Cranial Anatomy of *Acrocanthosaurus atokensis* and Its Implications for the Phylogeny of Allosauroidea (Dinosauria: Theropoda)." *PloS ONE* 6, no. 3 (March 21): e17932. https://doi.org/10.1371/journal.pone.0017932.

Foffa, Davide, Judyth Sassoon, Andrew R. Cuff, Mark N. Mavrogordato, and Michael J. Benton. 2014. "Complex Rostral Neurovascular System in a Giant Pliosaur." *The Science of Nature—Naturwissenschaften* 101 (23 April): 453–456.

Ford, Tracy L. 1997. "Did Theropods have Lizard Lips?" In *Proceedings of the Southwest Paleontological Symposium*. Edited by B. Anderson, D. Boaz, and R. D. McCord, 65–78. Mesa, Arizona: Mesa Southwest Museum.

Foth, Christian, Serjoscha W. Evers, Ben Pabst, Octávio Mateus, Alexander Flisch, Mike Patthey, and Oliver W.M. Rauhut. 2015. "New Insights into the Lifestyle of *Allosaurus* (Dinosauria: Theropoda) Based on Another Specimen with Multiple Pathologies." *PeerJ* 3 (May12): e940. https://doi.org/10.7717/peerj.940.

Gilmore, Charles Whitney. 1920. "Osteology of the Carnivorous Dinosauria in the United State National Museum, With Special Reference to the Genera Antrodemus (*Allosaurus*) and *Ceratosaurus*." *Bulletin (United States National Museum)*, 110. Washington, DC: Smithsonian Intituition United States Museum.

Hamm, C.A., O. Hampe, D. Schwarz, F. Witzmann, P.J. Makovicky, C.A. Brochu, R. Reiter, and P. Asbach. 2020. "A Comprehensive Diagnostic Approach Combining Phylogenetic Disease Bracketing and CT Imaging Reveals Osteomyelitis in a *Tyrannosaurus rex*." *Scientific Reports* 10 (3 November). https://doi.org/10.1038/s41598-020-75731-0.

Hendrickx, Christophe, Octávio Mateus, and Ricardo Araújo. 2015. "A Proposed Terminology of Therapod Teeth (Dinosauria, Saurischia)." *Journal of Vertebrate Paleontology* 35, no. 5 (1 September): 1–18. doi:10.1080/02724634.2015.982797.

Ibrahim, Nizar, Paul C. Sereno, Cristiano Dal Sasso, Simone Maganuco, Matteo Fabbri, David M. Martill, Samir Zouhri, Nathan Myhrvold, and Dawid A. Iurino. 2014. "Semiaquatic Adaptations in a Giant Predatory Dinosaur." *Science* 345, no. 6204 (11 September): 1613–1616.

International Commission on Zoological Nomenclature. 2023. "Opinion 2486 (Case 3506)—*Allosaurus* Marsh, 1877 (Dinosauria, Theropoda): Usage Conserved by Designation of a Neotype for its Type Species *Allosaurus fragilis* Marsh, 1877." *The Bulletin of Zoological Nomenclature* 80, no. 1 (29 December): 65–68.

Ketchum, Hilary F., and Adam S. Smith. 2010. "The Anatomy and Taxonomy of *Macroplata tenuiceps* (Sauropterygia, Plesiosauria) from the Hettangian (Lower Jurassic) of Warwickshire, United Kingdom." *Journal of Vertebrate Paleontology* 30, no. 4 (13 July): 1069–1081. https://doi.org/10.1080/02724634.2010.483604.

Laurenti, Josephi Nicolai. 1768. *Specimen Medicum, Exhibens Synopsin Reptilium Emendatam cum Experimentis Circa Venena [Medical Specimen: Presenting an improved synopsis of reptiles with experiments on poisons]*. Vienna. Austria: Joan. Thom. Nob. de Trattern.

Lautenschlager, Stephan. 2015. "Estimating Cranial Musculoskeletal Constraints in Theropod Dinosaurs." *Royal Society Open Science* 2, no. 11 (November): 150495. doi:https://doi.org/10.1098/rsos.150495.

Leitch, Duncan B., and Kenneth C. Catania. 2012. "Structure, Innervation and Response Properties of Integumentary Sensory Organs in Crocodilians." *Journal of Experimental Biology* 215, no. 23 (December 1): 4217–4230.

Lessner, Emily J., Corrine Cranor, Rebecca Hunt-Foster, and Casey M. Holliday. 2023. "Endocranial Anatomy of *Allosaurus* Supports Neural Trends Among Non-Avian Theropod Dinosaurs." *Journal of Vertebrate Paleontology* 43, no. 1 (21 August): e2236161. https://doi.org/10.1080/02724634.2023.2236161.

Lomax, Dean R., Laura B. Porro, and Nigel R. Larkin. 2019. "Descriptive Anatomy of the Largest Known Specimen of *Protoichthyosaurus prostaxalis* (Reptilia: Ichthyosauria) Including Computed Tomography and Digital Reconstruction of a Three-Dimensional Skull." *PeerJ* 7 (January 8): e6112. https://doi.org/10.7717/peerj.6112.

Madsen, James H. Jr. 1976. "*Allosaurus Fragilis*: A Revised Osteology." *Bulletin (Utah Geological and Mineral Survey)* 109: 1–175.

Madsen, James H., and Samuel P. Welles. 2000. Ceratosaurus *(Dinosauria, Theropoda) A Revised Osteology*. Miscellaneous Publication 00 2, Utah Geological Survey.

Magovern, Charles. 2003. *Complete Self-Contained Valuation Document Skull Creek Basin Allosaurus* sp. Unpublished Appraisal. Boulder, Colorado: Stone Company.com.

Marsh, Othniel C. 1877. "Notice of New Dinosaurian Reptiles from the Jurassic Formation." *American Journal of Science* s3–14, no. 84 (December 1): 514–516.

Marsh, Othniel Charles. 1878. "Notice of New Dinosaurian

Reptiles." *American Journal of Science* s3–15, no. 87 (March 1): 241–244.

Marsh, Othniel Charles. 1881. "Principal Characters of American Jurassic Dinosaurs. Part V." *American Journal of Science* s3–21, no. 125 (May 1): 417–423.

Mateus, Octávio. 2006. "Late Jurassic Dinosaurs from the Morrison Formation (USA), the Lourinhã and Alcobaça Formations (Portugal), and the Tendaguru Beds (Tanzania): A Comparison." *New Mexico Museum of Natural History and Science Bulletin* 36: 223–231.

McClelland, Brian Kent. 1990. "Anatomy and Kinesis of the Allosaurus Skull." Ph.D. diss. Texas Tech University.

McLain, Matthew, Matt Petrone, and Matthew Speights. 2018. "Feathered Dinosaurs Reconsidered: New Insights from Baraminology and Ethnotaxonomy." In *Proceedings of the Eighth International Conference on Creationism*. Edited by J.H. Whitmore, 472–515. Pittsburgh, Pennsylvania: Creation Science Fellowship.

Osmólska, Halszka. 1996. "An Unusual Theropod Dinosaur from the Late Cretaceous Nemegt Formation of Mongolia." *Acta Palaeontologica Polonica* 4, no. 1: 1–38.

Paul, Gregory S., and Kenneth Carpenter. 2010. "Case 3506 *Allosaurus* Marsh, 1877 (Dinosauria, Theropoda): Proposed Conservation of Usage by Designation of a Neotype for Its Type Species *Allosaurus Fragilis* Marsh, 1877." *The Bulletin of Zoological Nomenclature* 67, no. 1 (March): 53–56.

Porter, William Ruger, and Lawrence M Witmer. 2020. "Vascular Patterns in the Heads of Dinosaurs: Evidence for Blood Vessels, Sites of Thermal Exchange, and Their Role in Physiological Thermoregulatory Strategies." *The Anatomical Record* 303, no. 4 (April): 1075–1103.

Racicot, Rachel. 2016. "Fossil Secrets Revealed: X-Ray CT Scanning and Applications in Paleontology." *The Paleontological Society Papers. Virtual Paleontology* 22 (September): 21–38.

Rauhut, Oliver W.M., and Regina Fechner. 2005. "Early Development of the Facial Region in a Non-Avian Theropod Dinosaur." *Proceedings of the Royal Society B: Biological Sciences* 272, no. 1568 (7 June): 117–1183.

Reisz, Robert R., Diane M. Scott, Bruce R. Pynn, and Sean P. Modesto. 2011. "Osteomyelitis in a Paleozoic Reptile: Ancient Evidence for Bacterial Infection and Its Evolutionary Significance." *The Science of Nature—Naturwissenschaften* 98, no. 6 (June): 551–555.

Romer, Alfred Sherwood. 1956. *Osteology of the Reptiles*. Chicago, Illinois: Chicago University Press.

Ross, Marcus. 2014. "Ebenezer: AiG's *Allosaurus fragilis*." Unpublished Species Diagnosis.

Sampson, Scott D., and Lawrence M. Witmer. 2007. "Craniofacial Anatomy of *Majungasaurus crenatissimus* (Theropoda: Abelisauridae) from the Late Cretaceous of Madagascar." *Journal of Vertebrate Paleontology* 27, no. SP8 (June): 32–102.

Schumacher, Gert-Horst. 1973. "The Head Muscles and Hyolaryngeal Skeleton of Turtles and Crocodilians." In *Biology of Reptilia*. Vol. 4. *Morphology D.* Edited by Carl Gans, and Thomas S. Parsons, 101–199. London, United Kingdom: Academic Press.

Seeley, Harry Govier. 1888. "On the Classification of the Fossil Animals Commonly Named Dinosauria." *Proceedings of the Royal Society of London* 43, nos. 258–265 (31 December): 165–171.

Tanke, Darren, and Philip J. Currie. 1998. "Head-biting Behavior in Theropod Dinosaurs: Paleopathological Evidence." *GAIA—Ecological Perspectives for Science and Society* 15 (January): 167–184.

Van Loenen, R.E., and W. Anthony Bryant. 1999. "Geologic Map of the Skull Creek Quadrangle, Moffat County, Colorado." IMAP 2647. U.S. Geological Survey Publication. https://pubs.usgs.gov/imap/i-2647/I-2647.pdf.

Whitmore, John H, and Andrew A Snelling. 2014. "Ebenezer: Taphonomic Patterns in the Morrison Formation and a Recently Collected *Allosaurus* from Northwestern Colorado." *Journal of Creation Theology and Science Series C: Earth Sciences* 4, no. 2. https://www.coresci.org/jcts/index.php/jctsc/article/view/37.

Wilson, Jeffery A. 2006. "Anatomical Nomenclature of Fossil Vertebrates: Standardized Terms or 'Lingua Franca'?" *Journal of Vertebrate Paleontology* 26, no. 3 (September): 511–518.

Witmer, Laurence M. 1997a. "Craniofacial Air Sinus Systems." In *Encyclopedia of Dinosaurs*. Edited by Phillip J. Currie, and Kevin Padian, 151–159. San Deigo, California: Academic Press.

Witmer, Lawrence M. 1997b. "The Evolution of the Antorbital Cavity of Archosaurs: A Study in Soft-Tissue Reconstruction in the Fossil Record with an Analysis of the Function of Pneumaticity." *Journal of Vertebrate Paleontology* 17, sup001 (24 August): 1–76.